Spring 2012

Moxon based RFID tag reader and GPS antenna

Haojiong Liu
New Jersey Institute of Technology

Copyright Warning & Restrictions

The copyright law of the United States (Title 17, United States Code) governs the making of photocopies or other reproductions of copyrighted material.

Under certain conditions specified in the law, libraries and archives are authorized to furnish a photocopy or other reproduction. One of these specified conditions is that the photocopy or reproduction is not to be "used for any purpose other than private study, scholarship, or research." If a, user makes a request for, or later uses, a photocopy or reproduction for purposes in excess of "fair use" that user may be liable for copyright infringement,

This institution reserves the right to refuse to accept a copying order if, in its judgment, fulfillment of the order would involve violation of copyright law.

Please Note: The author retains the copyright while the New Jersey Institute of Technology reserves the right to distribute this thesis or dissertation

Printing note: If you do not wish to print this page, then select "Pages from: first page # to: last page #" on the print dialog screen

ABSTRACT

MOXON BASED RFID TAG READER AND GPS ANTENNA

by
Haojiong Liu

Modern communication applications at UHF frequencies require antennas with wide band, high forward gain, low backward radiation, high cross-polarization, small size and low manufacture cost. The Moxon antenna based on a two element Yagi-Uda antenna over the ground reflector is one of the most favorite antennas for HAM operators which can produce outstanding front to back ratio of radiated power, good match over the desired band and relatively low elevation height.

A sequence of topologies has been proposed from a single vertical element to two vertical elements of the Moxon arms, until the lately patented Broadband Circularly Polarized Moxon Based Antennas for UHF satellite communications (SATCOM). The logic was to obtain the best possible performance based on Fano-Chu limits for electrically small antenna with maximum radiating elements in a given volume. This dissertation is an extension of this configuration to cover Radio Frequency IDentification (RFID) (850 MHz-1050 MHz) and Global Positioning System (GPS) (centered at 1227 MHz and 1575 MHz) bands. Prototype antennas are built based on HFSS-11 simulations and experimental measurements yielded satisfactory results. Various design parameters of the proposed complex antenna are optimized to obtain a significant size reduction and much improved performance than the commercial counterpart antennas.

MOXON BASED RFID TAG READER AND GPS ANTENNA

by
Haojiong Liu

A Thesis
Submitted to the Faculty of
New Jersey Institute of Technology
in Partial Fulfillment of the Requirements for the Degree of
Master of Science in Electrical Engineering

Department of Electrical and Computer Engineering

May 2012

APPROVAL PAGE

MOXON BASED RFID TAG READER AND GPS ANTENNA

Haojiong Liu

Dr. Edip Niver, Thesis Advisor Professor of Electrical and Computer Engineering, NJIT	Date
Dr. Gerald Whitman, Committee Member Professor of Electrical and Computer Engineering, NJIT	Date
Dr. Ali N Akansu, Committee Member Professor of Electrical and Computer Engineering, NJIT	Date

BIOGRAPHICAL SKETCH

Author: Haojiong Liu

Degree: Master of Science

Date: May 2012

Undergraduate and Graduate Education:

- Master of Science in Electrical Engineering,
  New Jersey Institute of Technology, Newark, NJ, 2012

- Bachelor of Science in Electrical Engineering,
  University of Electronic Science and Technology of China, Chengdu, P. R. China, 2010

Major: Electrical Engineering

To my beloved family, teachers and friends

ACKNOWLEDGMENT

I would like to express my deepest appreciation to Professor Edip Niver. Dr. Niver served as my thesis advisor. He gave me the chance to do work on his recently developed concept and providing valuable insight and intuitions. He gave me constant support and encouragement throughout the whole year of my study. Researcher Oksana Manzhura helped me greatly during my thesis and her optimistic suggestions always encouraged me. Special thanks are given to Professor Gerald Whitman and Professor Ali N. Akansu for participating in my committee.

I also appreciate the support and help from my girlfriend Yuchen Guo and my friend Yuteng Zheng and Yifei Zhang.

Finally, all my special thanks to my beloved family for their endless support, love and belief in me.

TABLE OF CONTENTS

TABLE OF CONTENTS
(Continued)

Chapter **Page**

LIST OF TABLES

LIST OF FIGURES

LIST OF FIGURES
(Continued)

CHAPTER 1

INTRODUCTION

Antenna is commonly described as a transducer that converts electric currents/EM waves to EM waves/electric currents depending on being used in a transmitting/receiving mode. Modern applications of antennas encompass various functions, communication systems, radars, RFID, GPS are just few of the whole array of that is being used today. Various constraints and specifications arise depending on the needs of the particular application. Here, we focus on optimizing gain and bandwidth for reduced physical dimensions of the RFID tag reader and GPS antenna utilized in circular polarization excitation.

This work is an extension of the previously developed SATCOM antenna [1] based on Moxon antenna [2] to RFID and GPS frequency bands.

1.1 Antenna for Radio Frequency IDentification

Radio Frequency IDentification (RFID) is a wireless non-contact system use of radio frequency electromagnetic fields to probe remote tags to retrieve/change data for identification and tracking through a tag reader [3]. A basic RFID system consists of two elements, reader and tags. The reader is a scanner unit and the tags are sets of remote transponders which could either be passive or active. Every tag includes an antenna and a microchip transmitter with internal read/write memory. Tags could be classified as passive tags with no internal battery or as active tags with a battery. RFID technology has several standardized bands of operation. Ultra-high frequency (UHF, 815-860 MHz) band allows

longer communication ranges and smaller tags especially in sensor network applications. RFID antennas are usually designed based on several factors [4], such as operating frequency band, tag's reading distance from the reader, tag's known orientation to the reader, tag's arbitrary orientation to the reader, polarization of the reader antenna. Higher gain of the RFID Tag reader antenna is critical in increasing the physical range between the tag reader and the tag. Circular polarization of the tag reader antenna improves the overall reception due to tag antennas which are mostly linearly polarized.

1.2 Antenna for Global Positioning System

Global Positioning System (GPS) [5] is a space-based satellite navigation system that can provide location and time information. GPS system operates in dual frequency bands at L1 (1227.60 ± 10.23 MHz) and L2 (1575.42 ± 10.23 MHz) bands. L1 band is used for civilian purposes whereas L2 band is encrypted for demanding applications that require better accuracy and altitude information and primarily used by military. There are many important parameters such as gain, efficiency, radiation pattern and bandwidth that should be considered carefully for a successful GPS reception in terms of the signal to noise ratio performance at the receiver. A radiation pattern with a broad front lobe is required to obtain uniform coverage of necessary satellites. The radiation patter also should have a sharp slope for low elevation angles to avoid multipath and tropospheric effects. A high cross-polarization will also help to provide discrimination between the direct and reflect signals to eliminate the multipath effects.

This thesis is divided into five chapters. Chapter 1 introduces the basic idea of antenna for RFID and GPS applications. Chapter 2 describes the principle of the Moxon

antenna (two element Yagi-Uda antenna). Chapter 3 includes the definition of electrically small antenna, the physical limitations for electrically small antenna and some miniaturization techniques. Chapter 4 is the procedure of simulation and results for the simulation and prototypes that have been built. It also contains some comparison between the antennas designed in the thesis and some other antennas that already in the practice. Chapter 5 summarizes conclusions.

CHAPTER 2

MOXON (TWO ELEMENT YAGI-UDA) ANTENNA

2.1 Introduction

Yagi-Uda antenna is a kind of directional antenna consist one driven element (usually a dipole) and additional parasitic elements (reflector and one or more directors). The reflector element is longer than the driven dipole and the director elements are shorter than the driven dipole. Direction of radiation is from the reflector towards the driven element and the director(s). Yagi-Uda antenna is popular because of its highly directional properties and high gain. However, this high gain can only be achieved in a narrow range of the specified bandwidth.

2.2 Yagi-Uda Antenna: Two Elements

A two element Yagi-Uda antenna consist two parallel dipoles with a distance d apart. One connected to the source and the other shorted. The geometry is shown in Figure 2.1. [6]

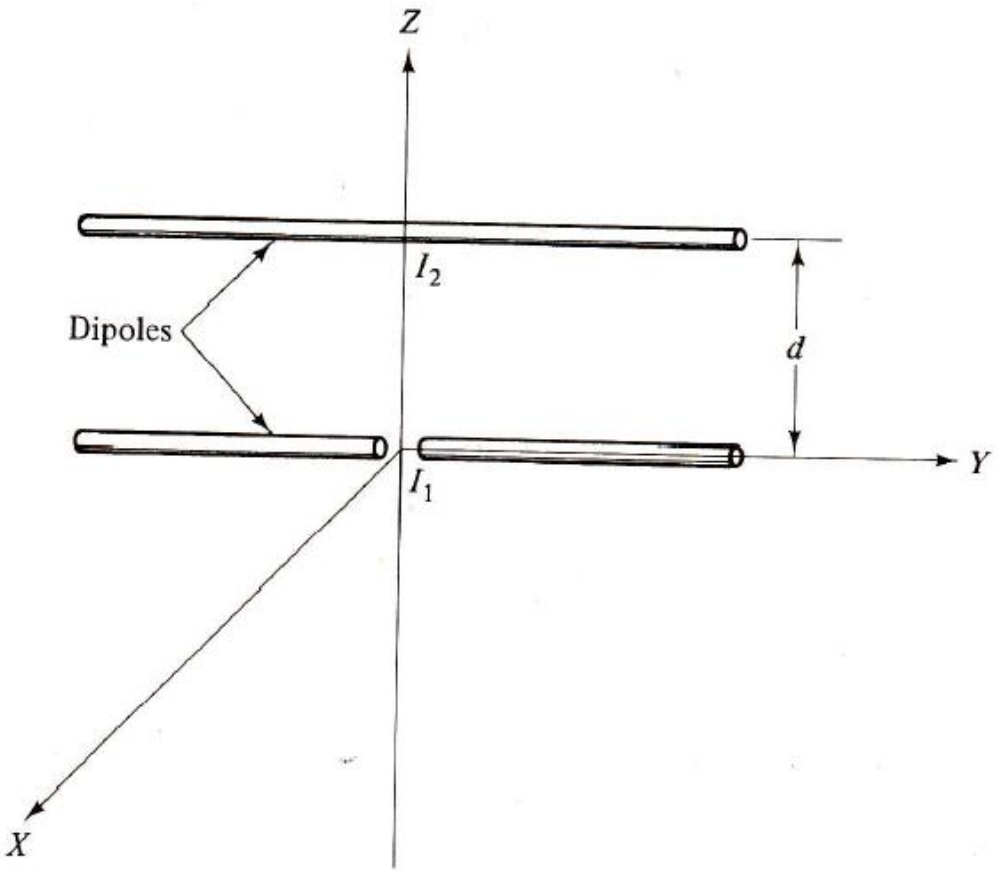

Figure 2.1 An array of two parallel dipoles, one driven, and one parasitic [6].

The mesh equations for this array are

$$\begin{aligned} V_1 &= I_1 Z_{11} + I_2 Z_{12} \\ 0 &= I_1 Z_{21} + I_2 Z_{22} \end{aligned} \tag{2.1}$$

and

$$\frac{I_2}{I_1} = -\frac{Z_{12}}{Z_{22}} \tag{2.2}$$

Since the array factor is given by

$$\alpha(\theta) = 1 + \frac{I_2}{I_1} e^{jkd\cos\theta} \tag{2.3}$$

One can obtain that the shape of the pattern is dominated by the spacing d/λ and by $-Z_{12}/Z_{22}$. It is also known that if the lengths of the two dipoles are near first resonance, the phase of the mutual impedance as a function of d/λ can be ignored because it is quite insensitive to the value of $2l_1/\lambda$ and $2l_2/\lambda$. So that the phase of I_2/I_1, is controlled by the phase of Z_{22} as shown in (2.2).

From the derivation of two parallel dipoles, the mutual impedance Z_{12} can be obtained with equation (2.4) and (2.5):

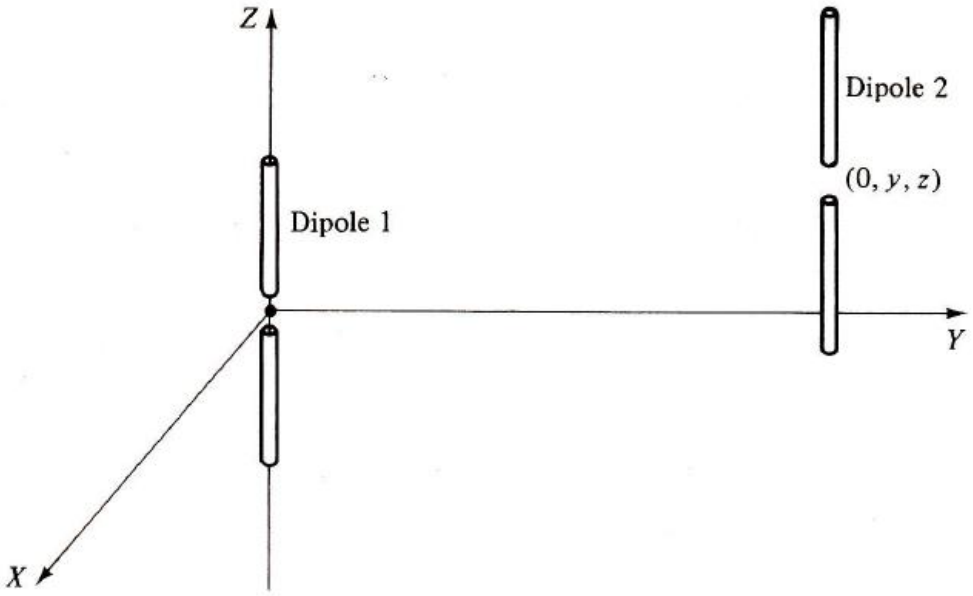

Figure 2.2 Two parallel Dipoles [6].

$$R_{12} = \frac{30}{\sin kl_1 \cdot \sin kl_2} \int_{-l_2/\lambda}^{l_2/\lambda} \left(\frac{\sin kr_1}{r_1/\lambda} + \frac{\sin kr_2}{r_2/\lambda} - 2\cos kl_1 \frac{\sin kr}{r/\lambda}\right) \cdot \sin k(l_2 - |\xi_2|) d\left(\frac{\xi_2}{\lambda}\right) \qquad (2.4)$$

$$X_{12} = \frac{30}{\sin kl_1 \cdot \sin kl_2} \int_{-l_2/\lambda}^{l_2/\lambda} \left(\frac{\cos kr_1}{r_1/\lambda} + \frac{\cos kr_2}{r_2/\lambda} - 2\cos kl_1 \frac{\cos kr}{r/\lambda}\right) \cdot \sin k(l_2 - |\xi_2|) d\left(\frac{\xi_2}{\lambda}\right) \qquad (2.5)$$

Where (0, y, z+ ξ_2) is the position of a point on the axis of dipole 2 with the central point of dipole 2 at the arbitrary position (0, y, z) in the YZ-plane, and dipole 1 is centered at the origin.

Z_{22} can also be obtained using King-Middleton second-order solution (2.6) and (2.7):

$$R(kl, \frac{a}{\lambda}) = \sum_{m=0}^{4} \sum_{n=0}^{4} a_{mn} (kl)^m (\frac{a}{\lambda})^n \tag{2.6}$$

$$X(kl, \frac{a}{\lambda}) = \sum_{m=0}^{4} \sum_{n=0}^{4} b_{mn} (kl)^m (\frac{a}{\lambda})^n \tag{2.7}$$

Where a/λ is the normalized radius, a_{mn} and b_{mn} are expansion coefficients.

Since the goal is to obtain an end-fire pattern with this two element Yagi-Uda antenna, if $2l_1/\lambda$ is given, one can seek if there are combinations of d/λ and $2l_2/\lambda$ which will enhance end-fire radiation.

As the input impedance often desired to be pure real, it is needed to adjust the ratio of $2l_1/\lambda$. From (2.1),

$$Z_{IN} = \frac{V_1}{I_1} = Z_{11} + \frac{I_2}{I_1} Z_{12} = Z_{11} - \frac{Z_{12}^2}{Z_{22}} \tag{2.8}$$

The imaginary part of Z_{11} and the imaginary part of $-Z_{12}^2 / Z_{22}$ has to cancel each other. For a two element Yagi-Uda antenna, a forward optimum and a rearward optimum cannot be achieved at the same spacing. Examples of forward radiation and rearward radiation are shown in Figure 2.3:

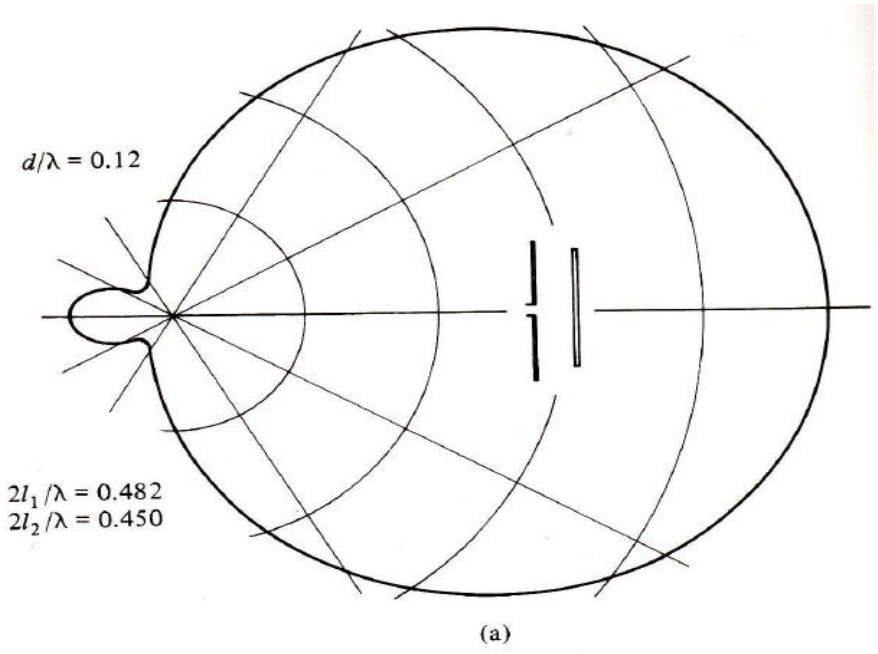

Figure 2.3 (a) H-Plane Power Patterns for Two-Element Yagi-Uda Arrays (forward) [6].

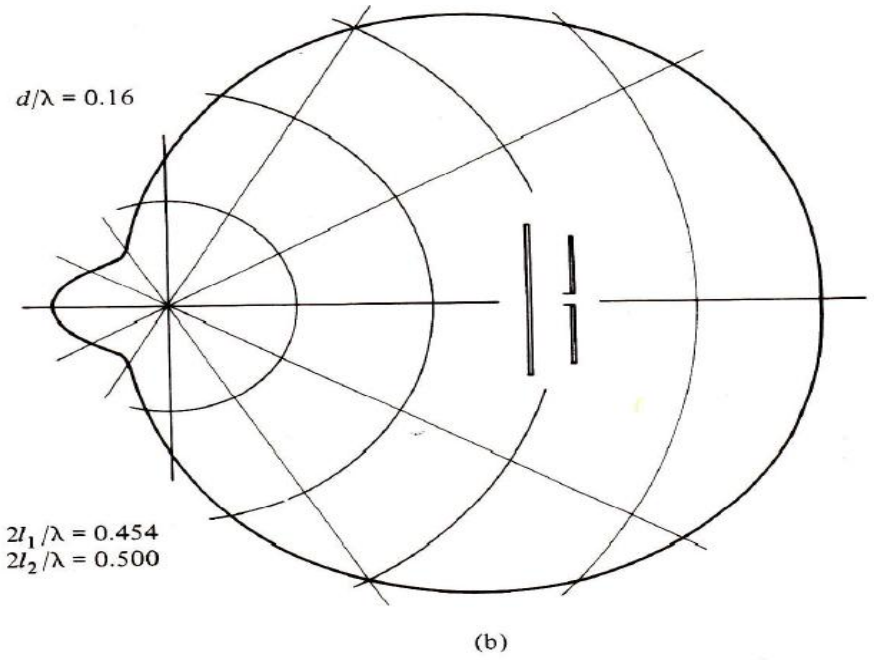

Figure 2.3 (b) H-Plane Power Patterns for Two-Element Yagi-Uda Arrays (rearward) [6].

Moxon antenna [1] is an extension of the two element Yagi-Uda array where linear dipole is bent over the reflector (ground). Such a combination results in higher forward gain, weak back lobe radiation and uniform impedance over a sufficient bandwidth.

CHAPTER 3

ELECTRICALLY SMALL ANTENNA

3.1 Electrically Small Antenna

Electrically small antenna has been an attractive feature for numerous applications where the largest dimension of the antenna is no more than one-tenth of the wavelength [7]. However, this constraint could be relaxed further to maximum physical dimensions of less than half a wavelength. It is almost always desirable to have a smaller antenna without compromising the performance. Electrically small antenna has various applications in HF and VHF bands for tactical radios for mobile use, SATCOM antennas on broad of vehicles, helicopters and ships are just few worth to mention. Performance limitations such as gain and efficiency become obvious as antenna dimensions get smaller followed by impedance match over the desired frequency band. Most applications are embedded in the environment with a finite ground plane resulting in back lobe radiation as well as reduced cross-polarization. Considering above parameters Moxon antenna [1] has been very popular among the HAM operators worldwide. Moxon antenna is known for its compact size and its directive properties due to the presence of the ground plane. Keeping in mind the physical constraints placed as Fano-Chu limits for electrically small antennas [8]-[9] resulting in electrically small antenna with maximum radiating elements in a given volume.

3.2 Physical Limitations of Omnidirectional Antenna

Electrically small antennas pose a major problem in regard to their electrical performance [10]. The radiation resistance of these antennas decreases rapidly with decreasing size but have a large reactive component, that makes the matching very difficult and inefficient due to the significant impedance of large reactive component in the system that contributes to system loss. As a consequence, the antenna performance parameters such as radiation efficiency, S/N-ratio, and bandwidth tend to deteriorate to unacceptable levels.

The limitations of omnidirectional antennas are estimated based on the following three criteria:

- Maximum gain (G) for a given complexity of the antenna structure,
- Minimum Q,
- Maximum ratio of G/Q.

3.2.1 Field of a Vertically Polarized Omnidirectional Antenna

Consider the field of a vertically polarized omnidirectional antenna lies totally within a spherical surface of a radius a. Under the spherical coordinate system (R,θ,ϕ), with an arbitrary current distribution and antenna structure, the three non-vanishing field components can be expressed in terms of a complete set of orthogonal, spherical waves, propagating radially outward. For a vertically polarized omnidirectional antenna, only TM modes exit.

$$
\begin{aligned}
H_{\phi} &= \sum_{n} A_n P_n^{1}(\cos\theta) h_n(kR) \\
E_R &= -j\sqrt{\frac{\mu}{\varepsilon}} \sum_{n} A_n n(n+1) P_n(\cos\theta) \frac{h_n(kR)}{kR} \\
E_{\theta} &= j\sqrt{\frac{\mu}{\varepsilon}} \sum_{n} A_n P_n^{1}(\cos\theta) \frac{1}{kR} \frac{d}{dR}[Rh_n(kR)]
\end{aligned}
\tag{3.1}
$$

where $P_n(\cos\theta)$ is the Legendre polynomial of order n, $P_n^1(\cos\theta)$ is the first associated Legendre polynomial, $h_n(kR)$ is the spherical Hankel function of the second kind, $k = \omega\sqrt{\mu\varepsilon} = 2\pi/\lambda$, $\sqrt{\mu/\varepsilon}$ is the wave impedance of a plane wave in free space and $1/\sqrt{\mu\varepsilon}$ is the velocity of a plane wave in free space. A_n is a complex coefficients that can be determined from the boundary conditions if the antenna structure is given. In the equations, the time factor $e^{j\omega t}$ is omitted.

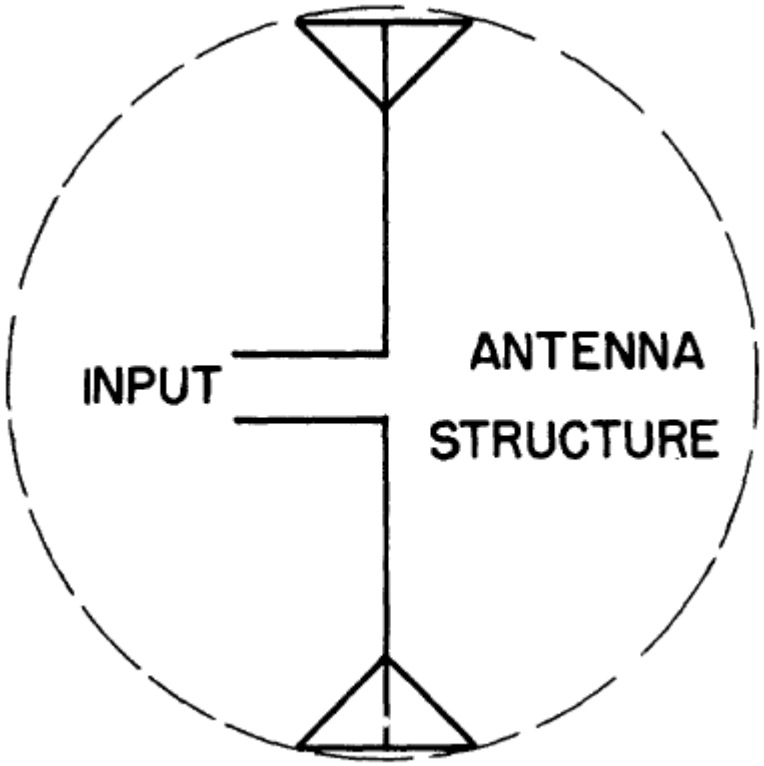

Figure 3.1 Schematic diagram of a vertically polarized omnidirectional antenna [10].

3.2.2 Far Field Characteristics

In the far field, the asymptotic field becomes

$$E_\theta = \sqrt{\frac{\mu}{\varepsilon}} \frac{e^{-jkR}}{kR} \sum_n A_n (-1)^{\frac{n+1}{2}} P_n^1(\cos\theta)$$
$$H_\phi = \sqrt{\frac{\varepsilon}{\mu}} E_\theta \tag{3.2}$$

by the definition of directivity gain,

$$G(\theta) = \frac{4\pi |E_\theta|^2}{\int_0^\pi \int_0^{2\pi} |E_\theta|^2 \sin\theta d\theta d\phi} = \frac{\left| \sum_n A_n (-1)^{\frac{n+1}{2}} P_n^1(\cos\theta) \right|^2}{\sum_n |A_n|^2 \frac{n(n+1)}{2n+1}} \tag{3.3}$$

The denominator is obtained from the orthogonality of the associated Legendre polynomials:

$$\int_0^\pi [P_n^1(\cos\theta)]^2 \sin\theta d\theta = \frac{2n(n+1)}{2n+1}$$

and

$$\int_0^\pi [P_n^1(\cos\theta)] P_n^{1\prime}(\cos\theta) \sin\theta d\theta = 0 \text{ for } n \neq n'$$

In the equatorial plane, $\theta = \pi/2$,

$P_n^1(0) = 0$ for n even and

$$P_n^1(0) = (-1)^{\frac{n-1}{2}} \frac{n!}{2^{n-1}(\frac{n-1}{2}!)^2} \text{ for n odd}$$

Thus all the even n terms have no contribution to the radiation field along the equator plane. To obtain a high directivity gain in the equatorial plane, it is necessary to have

$A_n = 0$ for n even

While all the A_n for odd n terms have the same phase angle. Consider all A_n to be positive real numbers for odd n and zero for even n, the directivity gain on the equatorial plane can be rewritten as

$$G(\frac{\pi}{2}) = \frac{[\sum A_n(-1)^{\frac{n+1}{2}} P_n^1(0)]}{\sum A_n{}^2 \frac{n(n+1)}{2n+1}} \tag{3.4}$$

3.2.3 Equivalent Circuits for Antenna

The complete equivalent circuit for the antenna is given in Figure 3.2.

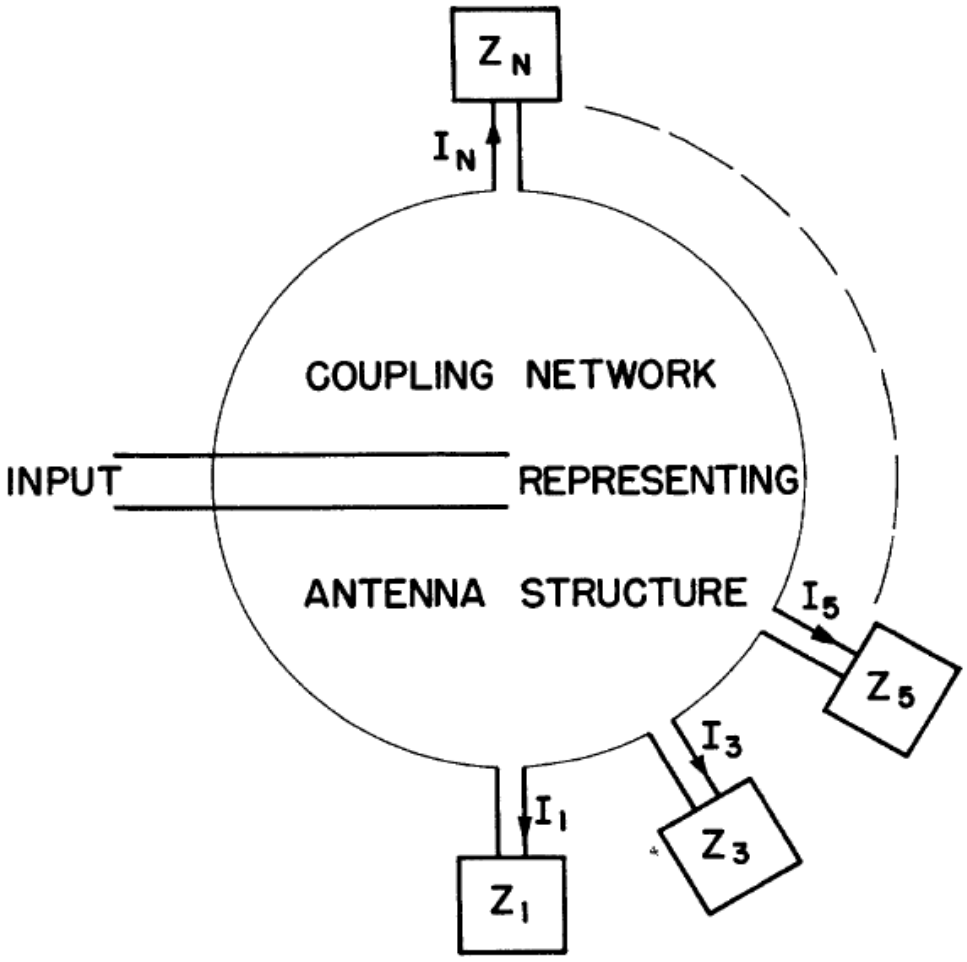

Figure 3.2 Equivalent circuit for a vertically polarized omnidirectional antenna [10].

The circular box is a coupling network that represents the space inside the geometrical sphere is shown in Figure 3.1. The input terminal represents the source of the antenna. Because of the orthogonal properties of the spherical waves, there will be no coupling between any two of the spherical waves outside the sphere. That means the total energy, electric or magnetic is equal to the sum of energies of each spherical wave component. In that case, it is possible to replace the space outside the sphere by a number of independent equivalent circuits, each with a pair of terminals connected to the box which represents the inside of the sphere. The number of the terminals is N+1 while N is the number of spherical waves used in describing the field outside the sphere.

The current, voltage, and impedance of the equivalent circuits are:

$$\begin{aligned} V_n &= 4\sqrt{\frac{\mu}{\varepsilon}}\frac{A_n}{k}\sqrt{\frac{4\pi n(n+1)}{2n+1}}\, j(\rho h_n)' \\ I_n &= 4\sqrt{\frac{\mu}{\varepsilon}}\frac{A_n}{k}\sqrt{\frac{4\pi n(n+1)}{2n+1}}\, \rho h_n \\ Z_n &= j(\rho h_n)'/\rho h_n \end{aligned} \tag{3.5}$$

where $\rho = ka$, $h_n = h_n(\rho)$, $(\rho h_n)' = \dfrac{d}{d\rho}\rho h_n(\rho)$.

The impedance Z_n can also be written as a continued fraction:

$$Z_n = \frac{n}{j\rho} + \cfrac{1}{\cfrac{2n-1}{j\rho} + \cfrac{1}{\cfrac{2n-3}{j\rho} + \ldots}} \tag{3.6}$$

This function represents a cascade circuit of series capacitances and shunt inductances terminated with a unit resistance. This circuit is shown in Figure 3.3.

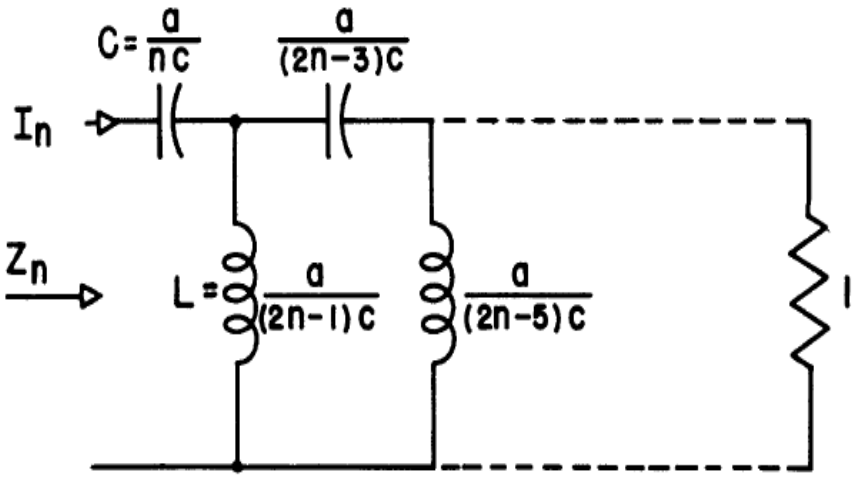

Figure 3.3 Equivalent circuit of Z_n [10].

The capacitances and inductances are proportional to the ratio of the radius of the sphere to the speed of light. To approximate the equivalent circuit of Z_n use simple RLC circuit that has the same frequency behavior of the operating frequency, R_n, C_n and L_n can be calculated by (3.7):

$$\begin{aligned} R_n &= \left|\rho h_n\right|^{-2} \\ C_n &= \frac{2}{\omega^2}\left[\frac{dX_n}{d\omega} - \frac{X_n}{\omega}\right]^{-1} \\ L_n &= \frac{1}{2}\left[\frac{dX_n}{d\omega} + \frac{X_n}{\omega}\right] \end{aligned} \tag{3.7}$$

where $X_n = [\rho j_n(\rho j_n)' + \rho n_n(\rho n_n)']\left|\rho h_n\right|^{-2}$, j_n and n_n are the spherical Bessel functions of the first and second kind.

The average power dissipation in Z_n and the average electric energy stored in Z_n can be obtained.

$$P_n = \sqrt{\frac{\mu}{\varepsilon}}\,\frac{2\pi n(n+1)}{2n+1}\left(\frac{A_n}{k}\right)^2 \tag{3.8}$$

$$W_n = \sqrt{\frac{\mu}{\varepsilon}}\,\frac{\pi n(n+1)}{2(2n+1)}\left(\frac{A_n}{k}\right)^2 \left|\rho h_n\right|^2 \left[\frac{dX_n}{d\omega} - \frac{X_n}{\omega}\right] \tag{3.9}$$

Define Q_n as

$$Q_n = \frac{2\omega W_n}{P_n} = \frac{1}{2}\left|\rho h_n\right|^2 \left[\rho \frac{dX_n}{d\rho} - X_n\right] \tag{3.10}$$

Assume there is no conduction loss in the antenna structure, there will be no electrical energy stored besides the form of travelling wave and the average magnetic energy stored beyond the terminals is equal to the average electric energy stored at operating frequency.

Now, define a quantity Q at the input terminals:

$$Q = \frac{2\omega \text{ times the mean electric energy stored beyond the input terminal}}{\text{power dissipated in radiation}}$$

In this case, if this Q is low, the input impedance of the antenna varies slowly with frequency, that means the antenna is potentially wideband. If it is high, the bandwidth of the antenna is equal to the reciprocal of Q.

Now, Q can be written as:

$$Q = \frac{\sum A_n^{\,2}\,\frac{n(n+1)}{2n+1}\,Q_n(\rho)}{\sum A_n^{\,2}\,\frac{n(n+1)}{2n+1}} \tag{3.11}$$

where Q_n is given in (3.10)

3.2.4 Criterion I: Maximum Gain

Whenever the antenna's structure is given, it is always demanded that the antenna can yield the possible maximum gain. Differentiating the gain in the equatorial plane, [Eq. (3.4)], with the respect to the coefficient A_n and setting the derivative to zero,

$$A_n = (-1)^{\frac{n+1}{2}} \frac{2n+1}{n(n+1)} P_n^1(0) \frac{\sum A_n^2 \frac{n(n+1)}{2n+1}}{\sum A_n (-1)^{\frac{n+1}{2}} P_n^1(0)}$$

Noticed that there are as many equations of this form as the number of terms in the A_n series, therefore, A_n can be solved in terms of the first coefficient A_1 as

$$A_n = (-1)^{\frac{n-1}{2}} \frac{2(2n+1)}{3n(n+1)} P_n^1(0) A_1 \tag{3.12}$$

Remember that $A_n = 0$ for n even, the corresponding gain and Q of the antenna will lead to

$$G(\frac{\pi}{2}) = \sum_1^N a_n \tag{3.13}$$

$$Q = \sum_1^N a_n Q_n / \sum_1^N a_n \tag{3.14}$$

where N is an odd integer indicate the order of the series, which represented the complexity of the source distribution, and

$$a_n = \frac{2n+1}{n(n+1)} [P_n^1(0)]^2 \tag{3.15}$$

Except for the first few terms,

$$a_n \cong 4/\pi \tag{3.16}$$

Under this criterion, the gain has no relationship with the size of the antenna. It indicates that an extremely high gain can be achieved by an infinite small antenna.

However, in Equation (3.14), the denominator has approximately equal amplitudes while the numerator is an ascending series of $(N+1)/2$ terms. For any given value of $2\pi a/\lambda$, Q_n increases with n at a rapid rate. When $2\pi a/\lambda$ greater than N, Q is of the

order of unity or less, indicating that the antenna potentially a broadband system. When $2\pi a/\lambda$ smaller than N, Q will rises rapidly as $2\pi a/\lambda$ decreases. The transition occurs at

$$2\pi a/\lambda \cong N \tag{3.17}$$

corresponding gain is

$$G \cong \frac{2}{\pi}\cdot\frac{2\pi a}{\lambda} = \frac{4a}{\lambda} \tag{3.18}$$

This gain is called the normal gain for omnidirectional antenna, and it is equal to the gain obtained from a current distribution of uniform amplitude and phase along a line of length 2a.

In Figure 3.4, curve I shows the normal Q for the omnidirectional antenna. Curve II shows a gain twice the normal gain. It is obvious that in order to make it happened, twice as many as terms are needed, and a high Q is required. The slop of curve II indicates the difficulty of getting additional gain as the normal gain increases.

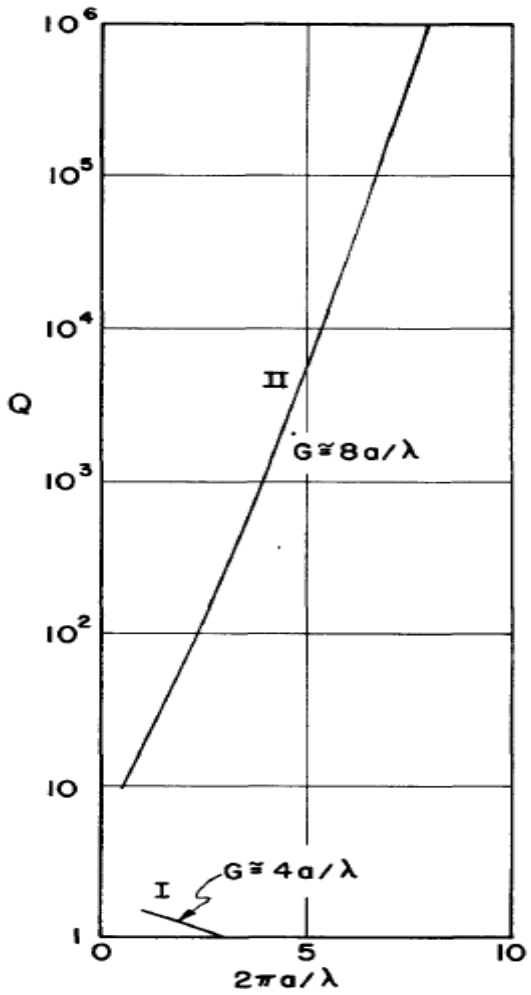

Figure 3.4 Q for omnidirectional antenna. Criterion: Max Gain with fixed number of terms. I normal gain. II twice the normal gain [10].

3.2.5 Criterion II: Minimum Q

Differentiating Q function with respect of A_n,

$$Q_n \sum A_n^2 \frac{n(n+1)}{2n+1} = \sum A_n^2 \frac{n(n+1)}{2n+1} Q_n$$

Q_n's will have different values when varies $2\pi a / \lambda$ are given. Hence the equation above can be satisfied when there is only one term under the summation sign. The Q of antenna is equal to the Q_n of the term used. Since Q_1 has the smallest amplitude, it can be

concluded that the infinitesimally small dipole has the potentially broadest bandwidth of all antennas. The gain of an infinite small antenna is 1.5.

3.2.6 Criterion III: Maximum G/Q

In most cases, it is impossible to give an infinite large Q in order to obtain a huge gain, and a gain of 1.5 is also not acceptable. Hence a compromise between maximum gain and minimum Q is required. So, the maximum ratio of the gain to Q is considered. The problem is to find a proper combination of A_n's for maximum G/Q.

Form Equations (3.4) and (3.11)

$$\frac{G}{Q} = \frac{[\sum A_n (-1)^{\frac{n+1}{2}} P_n^1(0)]^2}{\sum A_n^2 \frac{n(n+1)}{2n+1} Q_n} \tag{3.19}$$

With the same method used before,

$$A_n = (-1)^{\frac{n-1}{2}} \frac{2(2n+1)}{3n(n+1)} P_n^1(0) \frac{Q_1}{Q_n} A_1 \tag{3.20}$$

The corresponding values of G, Q and the ratio G/Q are:

$$G = \frac{[\sum a_n / Q_n]^2}{\sum a_n / Q_n^2} \tag{3.21}$$

$$Q = \frac{\sum a_n / Q_n}{\sum a_n / Q_n^2} \tag{3.22}$$

$$G / Q = \sum a_n / Q_n \tag{3.23}$$

where $a_n = \frac{2n+1}{n(n+1)} [P_n^1(0)]^2$.

In above equations, consider Q_n to be unity whenever its actual value is equal to or less than unity. Since the series in (3.21) and (3.22) converge rapidly as N increases, the

gain approaches asymptotically the value of $4a/\lambda$ which is the normal gain proven before. Curves of G/Q are shown in Figure 3.5. As in practical, it is always broadband is always wanted, that means Q is required to be low, so it is this physical limitation, among others, which limits the gain of antennas to the approximate value of $4a/\lambda$.

For horizontally polarized omnidirectional antenna, the analysis follows that of the vertically polarized antenna, and for circularly polarized antenna, it is a combination of both vertically polarized antenna and horizontally polarized antenna. The results for horizontal polarized antenna and circularly polarized antenna stay the same with the vertically polarized one. The conclusion is that in order to obtain a gain higher than the normal gain, it is a must to sacrifice the bandwidth under the most favorable conditions.

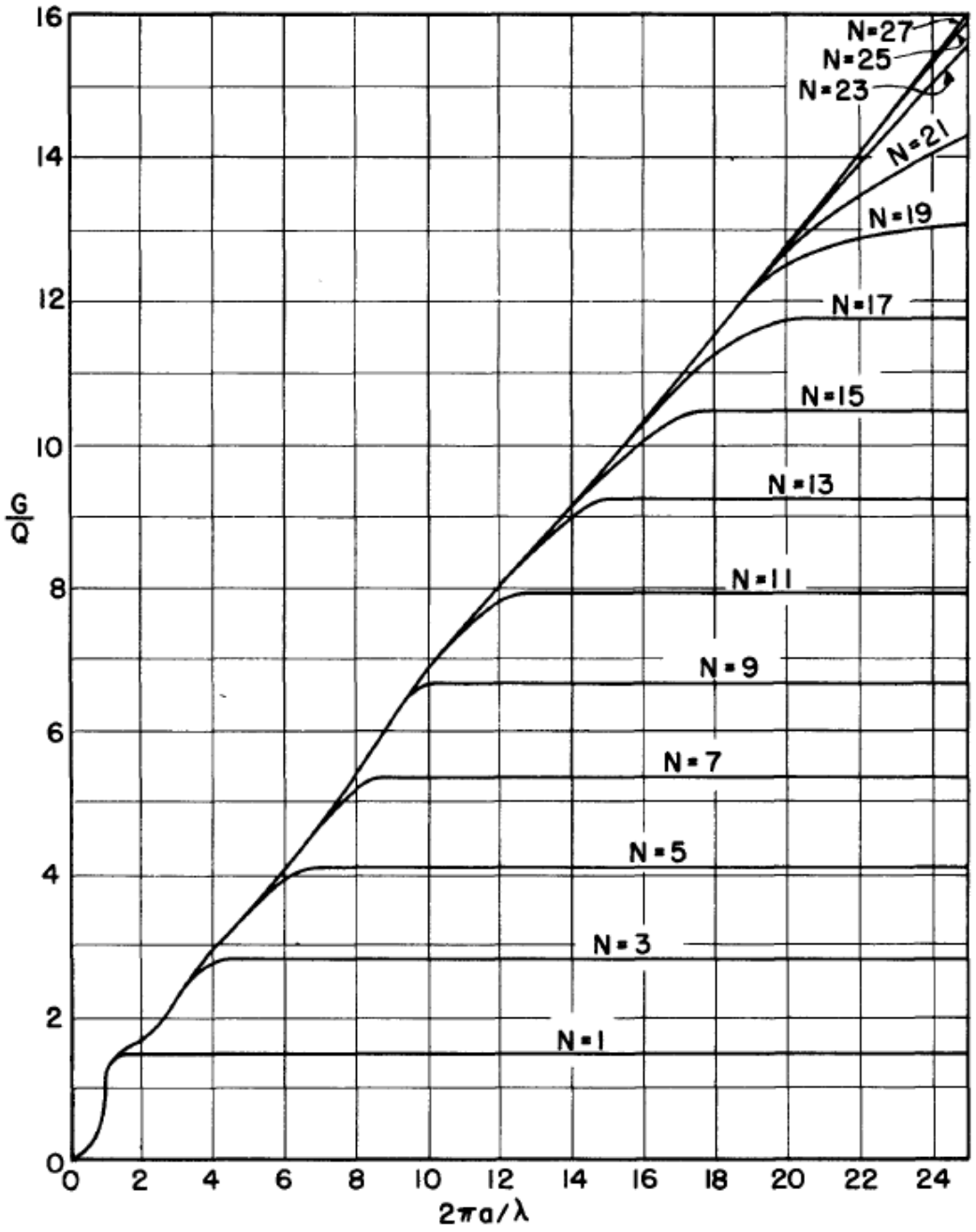

Figure 3.5 G/Q of omnidirectional antenna. Criterion: Max G/Q [10].

3.3 Other Limitations for Electrically Small Antennas

There are many other limitations for the electrically small antenna. In practical, the performance of antenna designed on the free space basis always will be affected by the

objects in the neighborhood. Objects nearby will give additional scattered radiation because of the induced current and also will distract the original current on the antenna structure. For bandwidth, it was interpreted freely as the reciprocal of the Q factor. But in real, the bandwidth can be increased by choosing a proper matching network.

3.4 Main Miniaturization Techniques Effect on the Performance [11]

In order to obtain better performance, there are several methods can be used in the real practice.

- Loading antenna with lumped elements. As we know that electrically small antenna will have a small radiation resistance and a strong reactive part of the impedance, it is logical to loading them reactively. A matching network will usually necessary to match the radiation resistance to the transmission line. The effect of loading antenna with lumped element will be, if the added element has losses, the efficiency will decreased, and if the added element is lossless, the antenna's quality factor will be enhanced which means the bandwidth will be reduced.
- Makes some parts of the antenna could be treated as virtual ground plane or equivalent short circuits may help to reduce the physical size.
- Optimizing the geometry of the antenna. This method contains geometrical loading with notches, slots… bend and curvature. Due to the current concentration, the efficiency will decrease and the bandwidth will be decreased due to frequency sensitivity of the technique.

Overall conclusion is that if the equivalent volume is filled with maximum number of radiating elements containing currents with uniform distributions, the antenna gain will be maximized.

This concept has been extended to Moxon antennas for SATCOM application [1].

CHAPTER 4

SIMULATION, EXPERIMENTAL RESULTS AND DISCUSSION

4.1 Simulation Procedures and Results

Moxon antenna is known for its compact size and its directive properties due to the presence of the ground plane; a sketch of the bent dipole antenna is shown in Figure 4.1 [1]. The length of the one arm of the dipole is L+W, and the arm is bended towards the ground from L distance away from the center of the dipole. The bottom of the dipole is H away from the ground plane. The bent dipole is fed with a input from the center. A circularly polarization can be achieved by placing two bent dipole antennas perpendicular to each other shown in Figure 4.2, one in x-z plane and the other in y-z plane and feeding though a hybrid quadrature coupler.

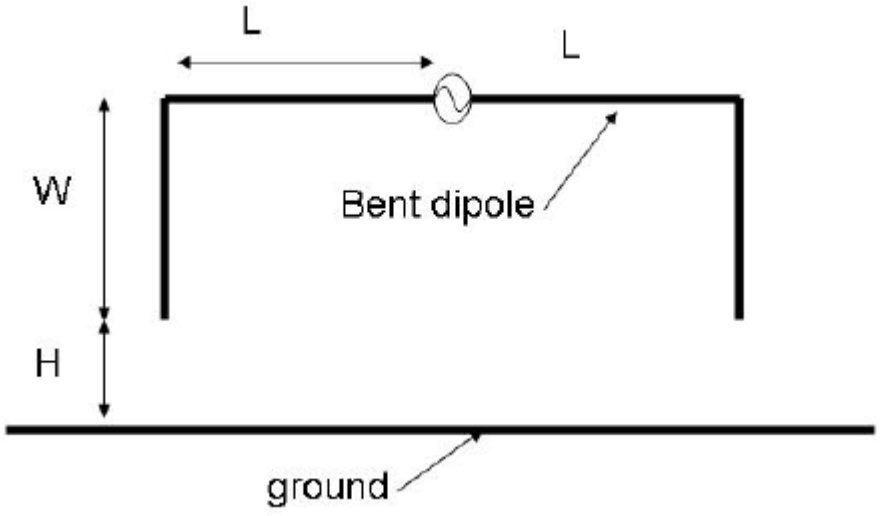

Figure 4.1 Moxon antenna [1].

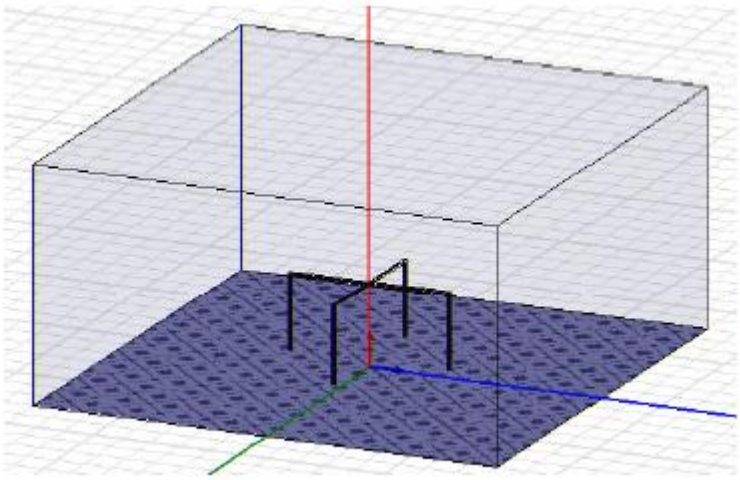

Figure 4.2 Two perpendicular Moxon antennas for circularly polarization radiation [1].

The first topology studied was a single vertical element Moxon antenna, and then two vertical elements Moxon antenna. After that, widened strip arm elements were investigated to understand its effects on increase of the bandwidth. This idea was based on Fano-Chu limits which indicate that more metallization in the radiating configuration that fill the volume would yield higher gain for electrically small antenna. Further, widening the strips lead to further improvement in the performance confirmed by Fano-Chu limits for electrically small antenna with maximum radiating elements in a given volume. Furthermore, splitting the tapered bow tie elements [12] increased the volume filled with radiating elements improved overall performance. Finally, bends at the tip of the tapered sections parallel to the ground pushing to optimized performance. During the simulation, great attention was paid on finding the effects on overall performance of each physical parameter of the antenna in terms of its dimensions and shape.

4.1.1 Simulation of RFID Antenna

The purpose of RFID antenna simulation was to obtain wider bandwidth, lower return loss, higher gain and better cross-polarization.

The operating frequency was first designed to be centered at 950 MHz, and then, every parameter of the antenna was carefully optimized separately to find its effect on the overall performance in terms of low frequency resonant point, high frequency resonant point, bandwidth, return loss S_{11} and gain of right hand circular polarization (RHCP). A summary is given at the end of this section. Ultimately, an optimized bent bow tie Moxon antenna for RFID at frequency range 850 MHz to 1050 MHz was obtained. The configuration of the optimized bent bow tie Moxon RFID antenna is given in Figure 4.3.

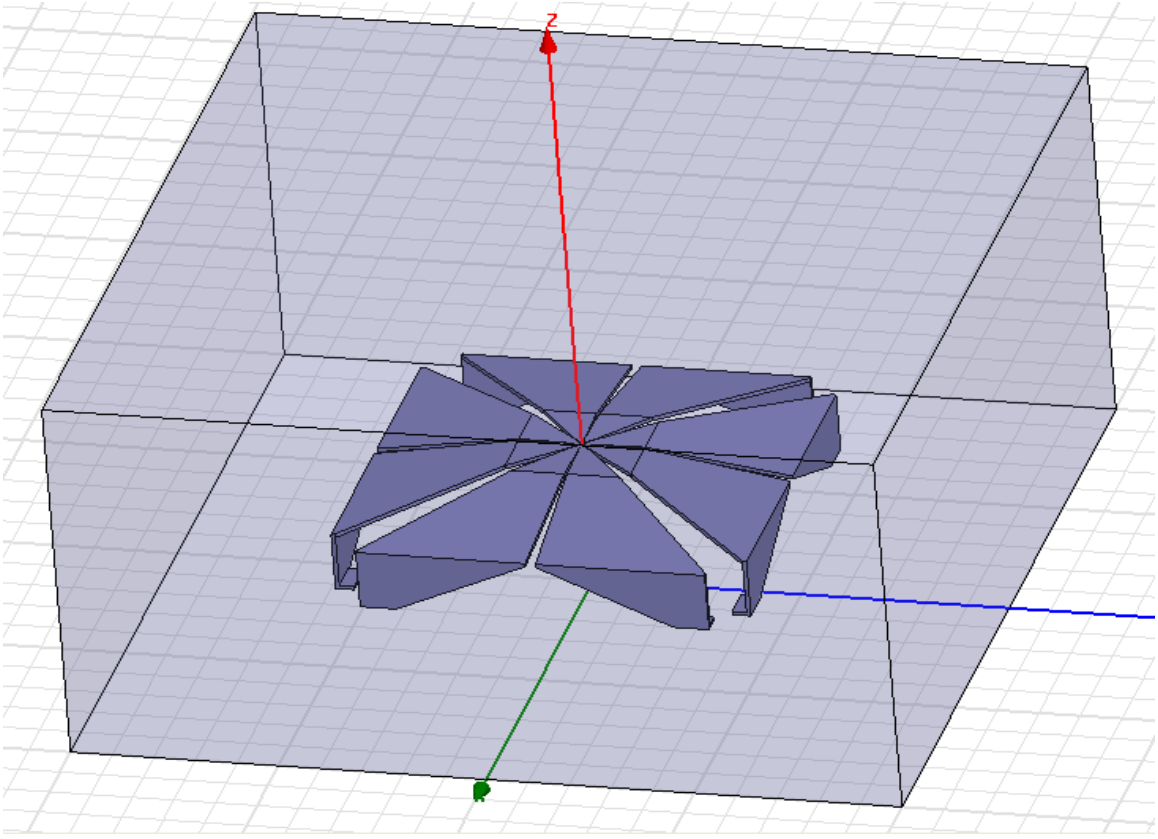

Figure 4.3 Bent bow tie antenna for RFID.

The total horizontal length of the antenna is 99.9 mm, the height from the top of the antenna to the ground plane is 40.0 mm, the bottom of the antenna to the ground plane is 18.0 mm, the cross section area (feeding area) is 1 mm × 1 mm.

The results of return loss (S_{11}), RHCP gain and radiation pattern at center frequency 950 MHz is given in Figure 4.4-4.6.

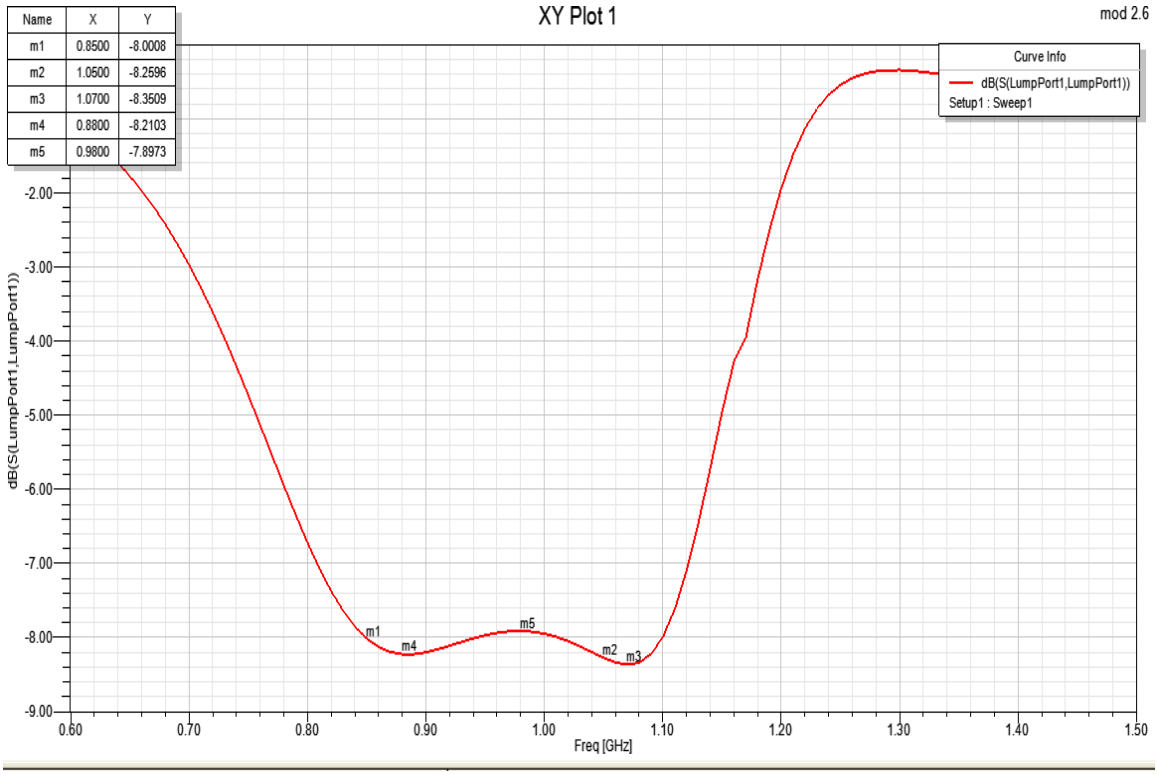

Figure 4.4 S_{11} of RFID antenna.

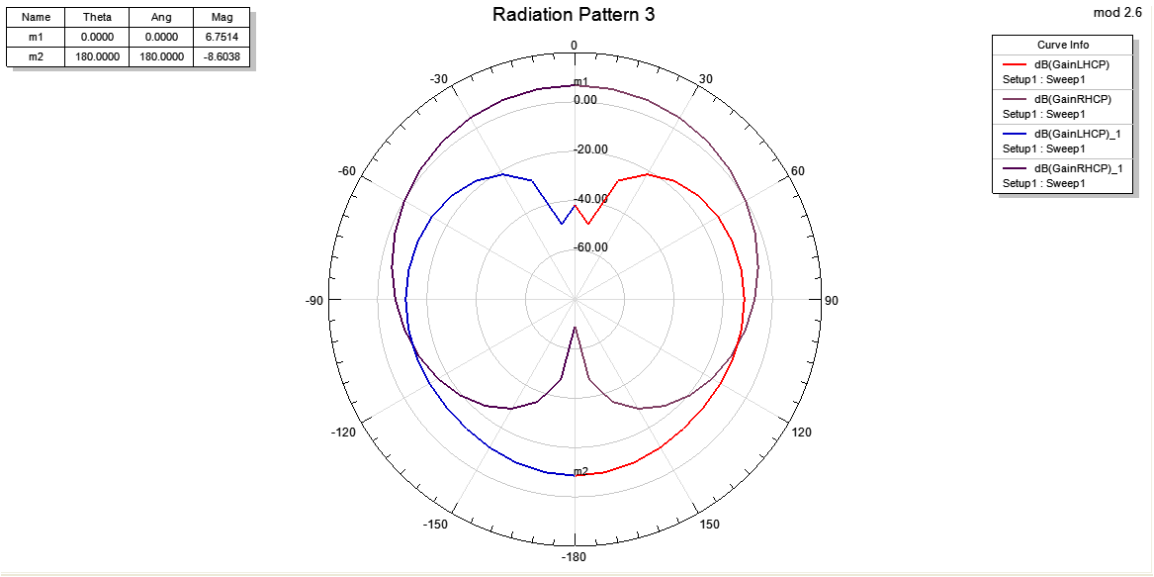

Figure 4.5 Gain of RHCP and radiation pattern at 950 MHz.

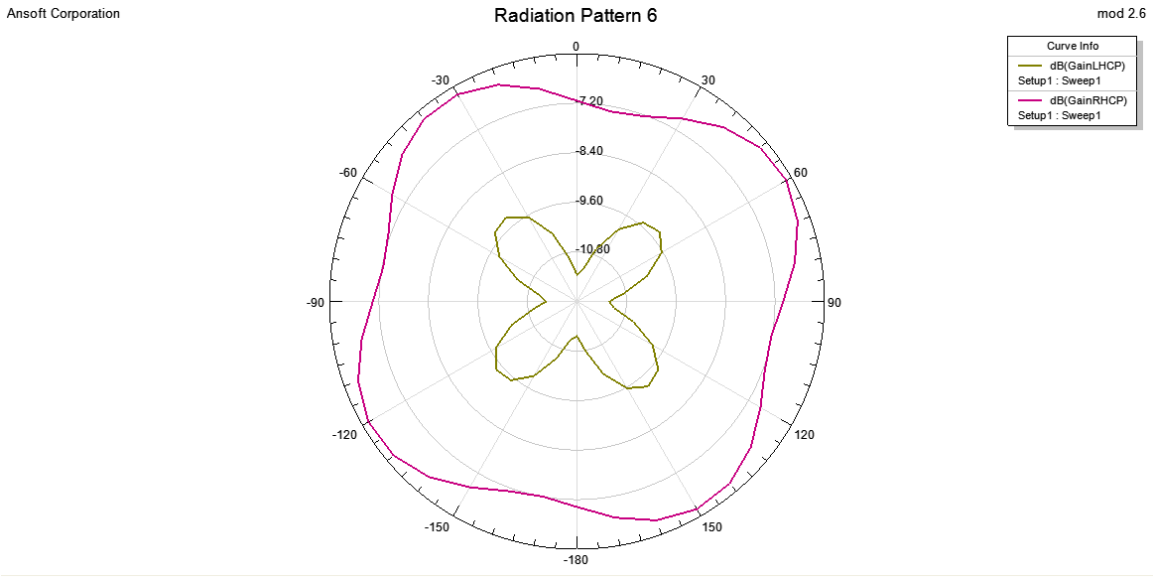

Figure 4.6 Radiation Pattern at 950 MHz.

From Figure 4.4, the optimized RFID antenna has a wide bandwidth from 850 MHz to 1100 MHz with a low return loss under -8 dB. From Figure 4.5, the gain for RHCP is about 6.75 dB and the cross polarization is about 15.35 dB. The antenna has no back scattering lobe and it has 80 degrees forward beam width with 3.5 dB due to infinite ground

plane consideration which requires much less computational effort compared to finite ground plane.

4.1.2 Simulation of GPS Antenna

For a GPS antenna, one of the cirtical requirements is design it at the proper frequency bands. GPS antenna has a dual band of operation; which are centered at 1227.60 ± 10.23 MHz and 1575.42 ± 10.23 MHz. High gain, low return loss, high cross-ploarization are also desired requirements for the GPS antenna.

First, the effect of every optimization parameter on overall performance was investigated as was done for the simulation of the RFID antenna. Most of the parameters behave same as for RFID antenna, but because the dimension of GPS antenna is smaller than RFID antenna, some parameters changed their behaviors, as shown the summary listed at the end of this section. Then, lower resonant frequency was set arround 1225 MHz while the higher resonant frequecy was set around 1570 MHz. The optimized results was very hard to obtain because the size of the GPS antenna was too small, even slight change of dimension will cause huge change in the overall performance. An optimized GPS antenna was finally obtained with two resonance points at 1228.0 MHz and 1575.2 MHz, which almost matches the ideal central operation frequencies of L1 and L2 bands.

The configuration of bent bow tie GPS antenna is given below:

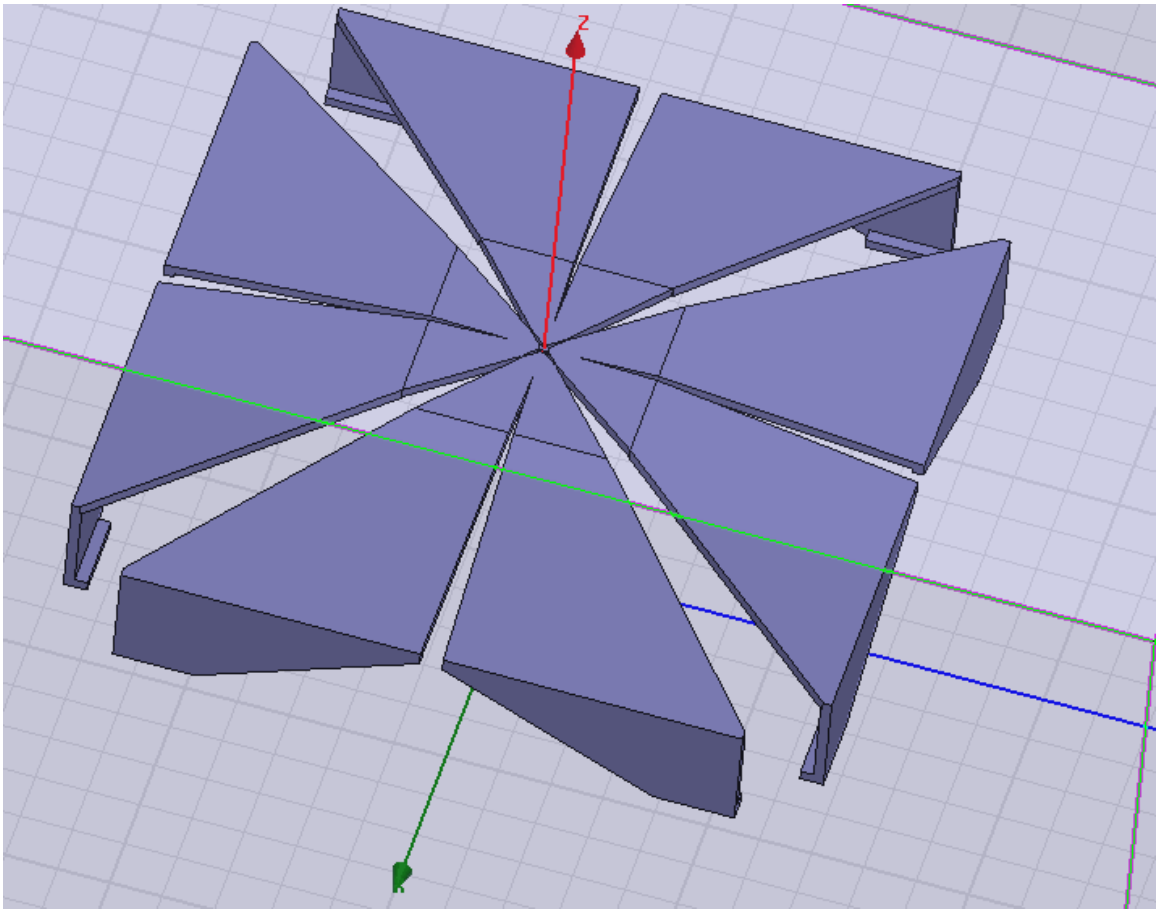

Figure 4.7 Bent bow tie antenna for GPS.

The total horizontal length of the antenna is 72.7 mm, the height from the top of the antenna to the ground plane is 30.0 mm, the bottom of the antenna to the ground plane is 15.3 mm, the cross section area (feeding area) is 1 mm × 1 mm.

The results of S_{11}, RHCP gain and radiation pattern at operation frequencies 1227 MHz and 1575 MHz are given in Figure 4.8-4.12.

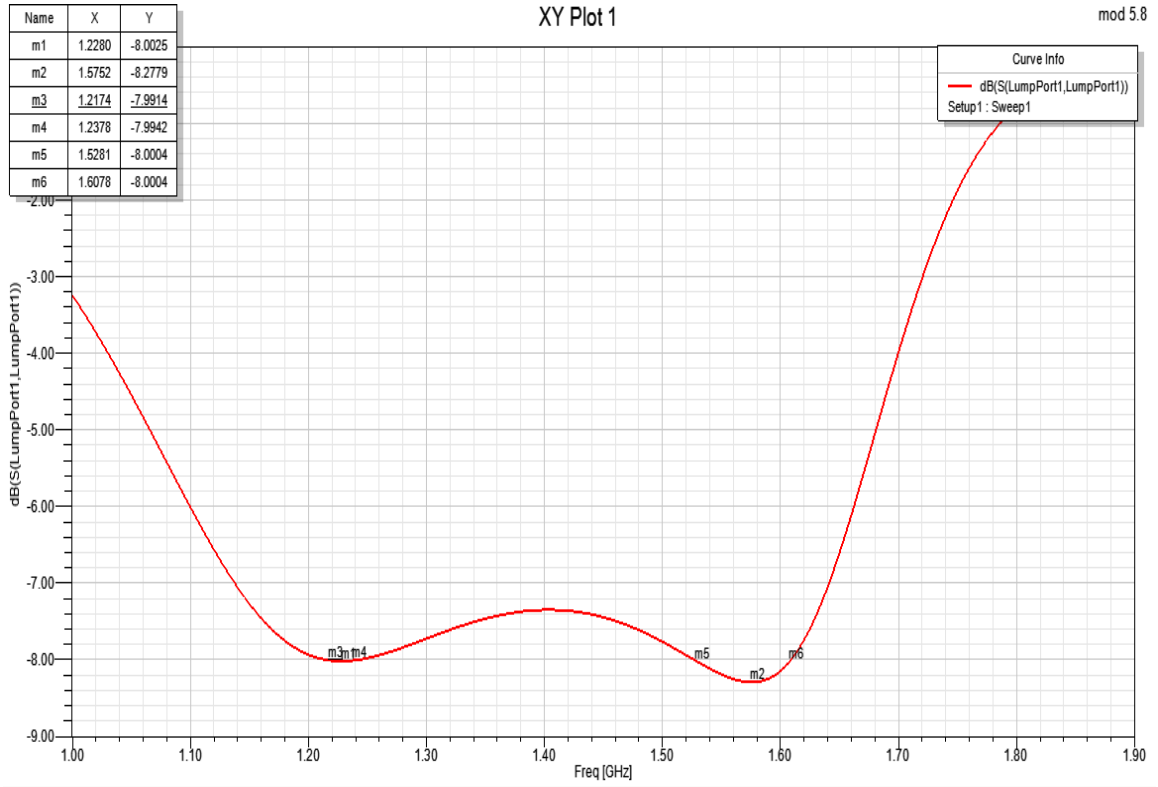

Figure 4.8 S_{11} of RFID antenna.

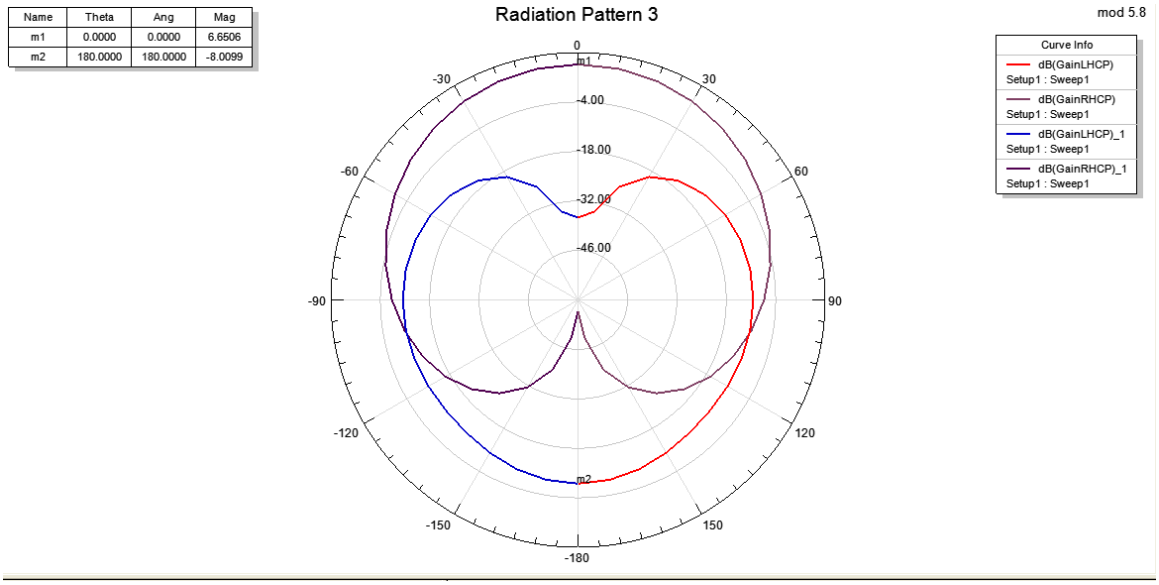

Figure 4.9 Gain of RHCP and radiation pattern at 1227 MHz.

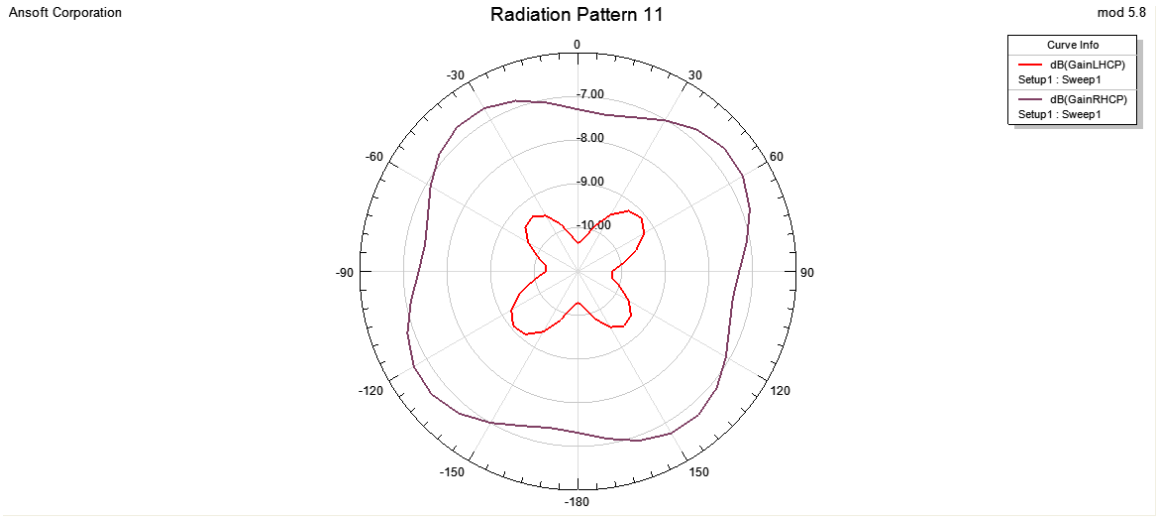

Figure 4.10 Radiation Pattern at 1227 MHz.

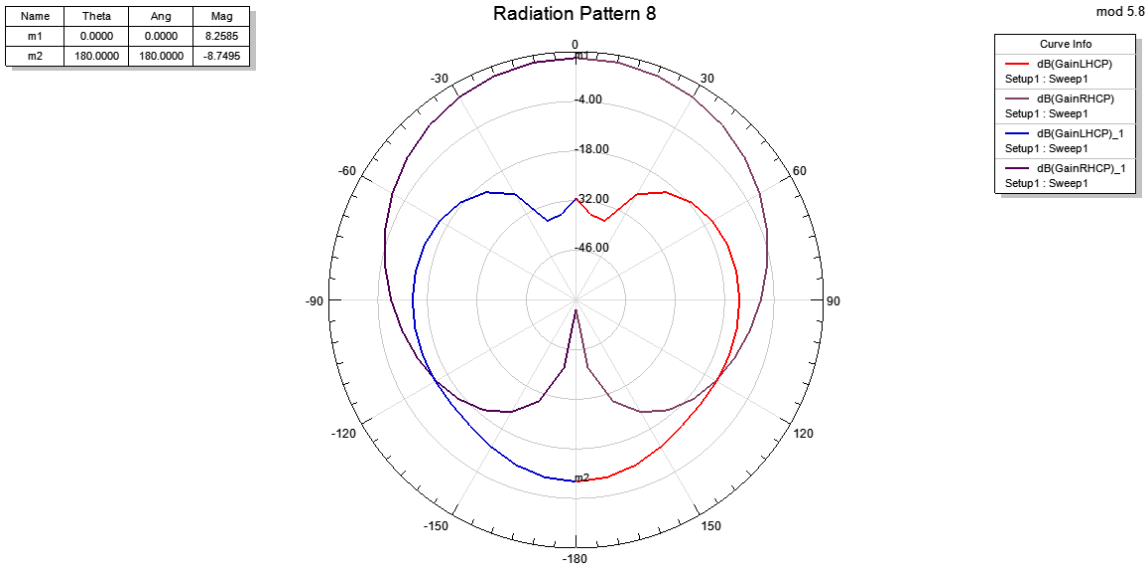

Figure 4.11 Gain of RHCP and radiation pattern at 1575 MHz.

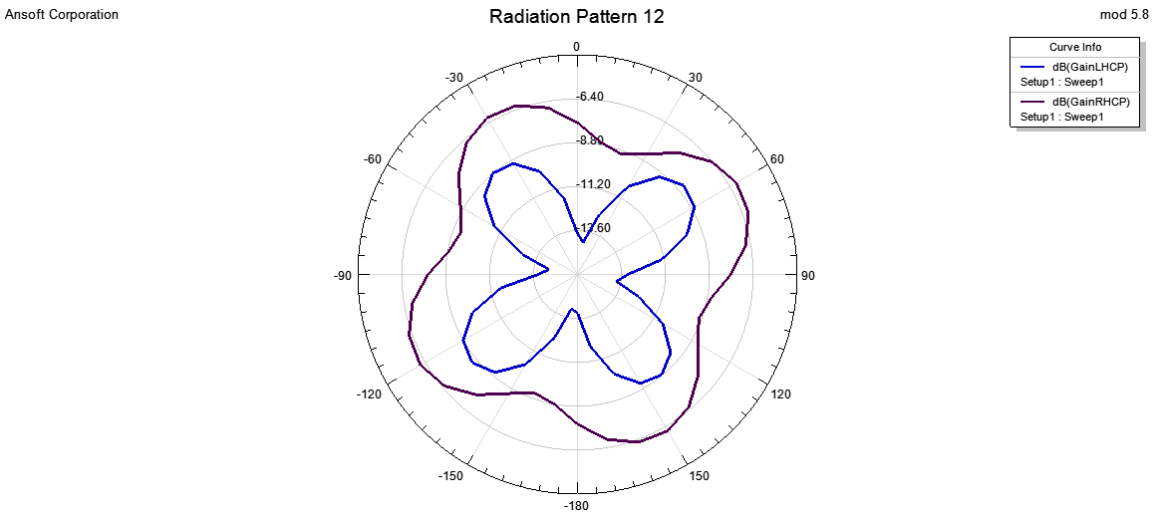

Figure 4.12 Radiation Pattern at 1575 MHz.

From Figure 4.8, the optimized antenna has wide bandwidth from 1217.4 MHz to 1237.8 MHz (20.4 MHz) and from 1528.1 MHz to 1607.8 MHz (79.7 MHz) for the two operation frequencies with a low return loss under -8 dB. From Figure 4.9 and Figure 4.11, the Gain for RHCP is about 6.65 dB at 1227 MHz and 8.26 dB at 1575 MHz, the cross polarization is about 14.65 dB at 1227 MHz and 17.0 dB and 1575 MHz, which are satisfactory requirements for a successful GPS antenna. Due to infinite ground plane considerations, the antenna has no back scattering lobe and it has 80 degrees forward beam width with 3.5 dB at 1227 MHz and 4.4 dB at 1575 MHz.

4.1.3 Optimization Parameters of the RFID Antenna

In order to clearly show the behavior of each optimization parameter's effect on the overall performance of the RFID antenna and GPS antenna, every parameter was numbered and shown in Figure 4.13

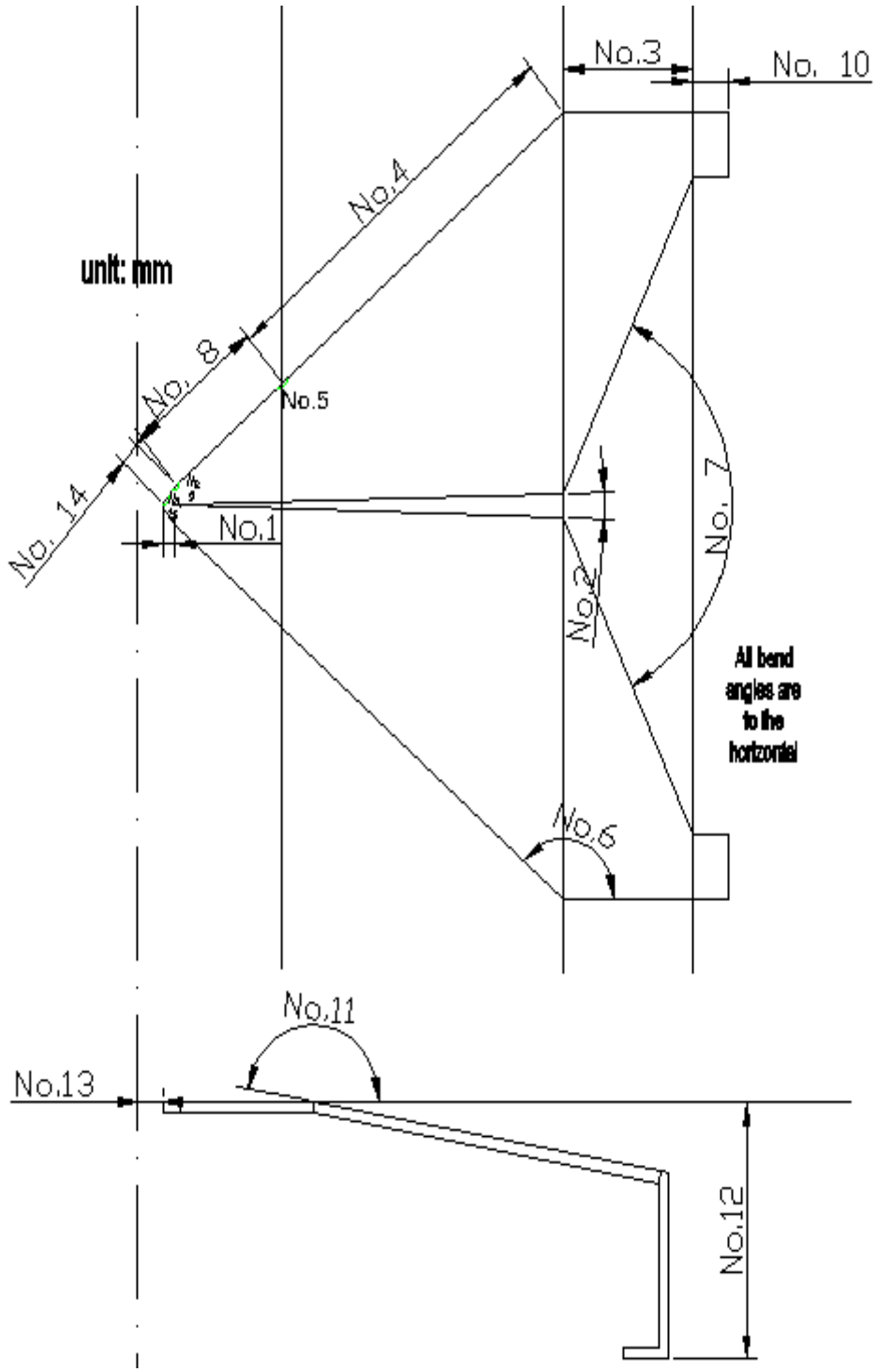

Figure 4.13 Antenna layout with optimization parameters numbered from 1 to 15.

The optimization parameters and their effect on the performance are outlined below for the RFID tag reader antenna:

No 1: Horizontal wedge position.

Away from the axis: Low resonance point stays in frequency but drops down in S_{11}, high resonance point moves higher in frequency and drops down in S_{11}. Total bandwidth increases.

Closer to the axis: Low resonance point stays in frequency but goes up in S_{11}, high resonance point moves lower in frequency and goes up in S_{11}. Total bandwidth decreases.

No 2: Horizontal wedge angle.

Bigger: Low resonance point stays in frequency but drops down in S_{11}, high resonance point moves lower in frequency and goes up in S_{11}. Total bandwidth decreases.

Sharpen: Low resonance point moves higher in frequency but goes up in S_{11}, high resonance point moves higher in frequency and drops down in S_{11}. Total bandwidth increases.

No 3: Vertical length (vertical section only).

Longer: Low resonance point moves lower in frequency but goes up in S_{11}, high resonance point moves lower in frequency and drops down in S_{11}. Total bandwidth decreases.

Shorter: Low resonance point movers higher in frequency but drops down in S_{11}, high resonance point moves higher in frequency and goes up in S_{11}. Total bandwidth increases.

No 4: Length of the first bend.

Longer: Low resonance point moves lower in frequency but goes up in S_{11}, high resonance point moves lower in frequency and goes up in S_{11}. Total bandwidth increases.

Shorter: Low resonance point moves higher in frequency but drops down in S_{11}, high resonance point moves higher in frequency and drops down in S_{11}. Total bandwidth decreases.

No 5: Outer angle of the first bend.

Bigger: Low resonance point moves lower in frequency but goes up in S_{11}, high resonance point moves lower in frequency and drops down in S_{11}. Total bandwidth decreases,

Sharpen: Low resonance point moves higher in frequency but drops down in S_{11}, high resonance point moves higher in frequency and goes up in S_{11}. Total bandwidth increases.

No 6: Outer angle of the vertical section. (In our case is 90 degrees)

It was observed that design was insensitive to the angular radiation.

No 7: Inner angle of the vertical section.

Bigger: Low resonance point moves lower in frequency but drops down in S_{11}, high resonance point moves lower in frequency and drops down in S_{11}. Total bandwidth stays.

Sharpen: Low resonance point moves higher in frequency but goes up in S_{11}, high resonance point moves higher in frequency and goes up in S_{11}. Total bandwidth stays.

No 8: Horizontal length (horizontal section only, no tip).

Longer: Low resonance point moves lower in frequency but goes up in S_{11}, high resonance point moves lower in frequency and drops down in S_{11}. Total bandwidth decreases.

Shorter: Low resonance point moves higher in frequency but drops down in S_{11}, high resonance point moves higher in frequency and goes up in S_{11}. Total bandwidth increases.

No 9: Outer angle of the horizontal section.

Bigger: Low resonance point moves higher in frequency but drops down in S_{11}, high resonance point moves lower in frequency and goes up in S_{11}. Total bandwidth decreases.

Sharpen: Low resonance point moves lower in frequency but goes up in S_{11}, high resonance point moves higher in frequency and drops down in S_{11}. Total bandwidth increases.

No 10: Length of the bottom bend.

Longer: Low resonance point stays in frequency but goes up in S_{11}, high resonance point moves higher in frequency and drops down in S_{11}. Total bandwidth increases.

Shorter: Low resonance point stays in frequency but drops down in S_{11}, high resonance point moves lower in frequency and goes up in S_{11}. Total bandwidth decreases.

No 11: First bend angle (vertical plane bend).

Bigger: Low resonance point moves higher in frequency but goes up in S_{11}, high resonance point moves higher in frequency and goes up in S_{11}. Total bandwidth decreases.

Smaller: Low resonance point moves lower in frequency but drops down in S_{11}, high resonance point moves lower in frequency and drops down in S_{11}. Total bandwidth increases.

No 12: Top to ground height.

Higher: Low resonance point moves higher in frequency but drops down in S11, high resonance point moves higher in frequency and drops down in S11. Total bandwidth increases.

Lower: Low resonance point moves lower in frequency but goes up in S_{11}, high resonance point moves lower in frequency and goes up in S_{11}. Total bandwidth decreases.

No 13: Half gap length.

Longer: Low resonance point moves lower in frequency but goes up in S_{11}, high resonance point moves higher in frequency and drops down in S_{11}. Total bandwidth increases.

Shorter: Low resonance point moves lower in frequency but drops down in S_{11}, high resonance point moves lower in frequency and goes up in S_{11}. Total bandwidth decreases.

No 14: Length of the tip.

Longer: Low resonance point moves lower in frequency but drops down in S_{11}, high resonance point moves lower in frequency and goes up in S_{11}. Total bandwidth decreases.

Shorter: Low resonance point moves higher in frequency but goes up in S_{11}, high resonance point moves higher in frequency and goes up in S_{11}. Total bandwidth increases.

No 15: Outer angle of the tip.

Bigger: Low resonance point moves higher in frequency but drops down in S_{11}, high resonance point moves lower in frequency and goes up in S_{11}. Total bandwidth decreases.

Sharpen: Low resonance point moves lower in frequency but drops down in S_{11}, high resonance point stays in frequency and goes up in S_{11}. Total bandwidth increases.

4.1.4 Optimization Parameters of the GPS Antenna

No 1: Horizontal wedge position.

Away from the axis: Low resonance point moves higher in frequency but goes up in S_{11}, high resonance point moves higher in frequency and drops down in S_{11}. Total bandwidth increases.

Closer to the axis: Low resonance point moves lower in frequency but drops down in S_{11}, high resonance point moves lower in frequency and goes up in S_{11}. Total bandwidth decreases.

No 2: Horizontal wedge angle.

Bigger: Low resonance point moves higher in frequency but drops down in S_{11}, high resonance point moves lower in frequency and goes up in S_{11}. Total bandwidth decreases.

Sharpen: Low resonance point moves lower in frequency but goes up in S_{11}, high resonance point moves higher in frequency and drops down in S_{11}. Total bandwidth increases.

No 3: Vertical length (vertical section only).

Longer: Low resonance point moves lower in frequency but goes up in S_{11}, high resonance point moves lower in frequency and drops down in S_{11}. Total bandwidth decreases.

Shorter: Low resonance point movers higher in frequency but drops down in S_{11}, high resonance point moves higher in frequency and goes up in S_{11}. Total bandwidth increases.

No 4: Length of the first bend.

Longer: Low resonance point moves lower in frequency but goes up in S_{11}, high resonance point moves lower in frequency and goes up in S_{11}. Total bandwidth decreases.

Shorter: Low resonance point moves higher in frequency but drops down in S_{11}, high resonance point moves higher in frequency and drops down in S_{11}. Total bandwidth increases.

No 5: Outer angle of the first bend.

Bigger: Low resonance point moves higher in frequency but drops down in S_{11}, high resonance point moves lower in frequency and drops down in S_{11}. Total bandwidth decreases,

Sharpen: Low resonance point moves lower in frequency but goes up in S_{11}, high resonance point moves higher in frequency and goes up in S_{11}. Total bandwidth increases.

No 6: Outer angle of the vertical section. (In our case is 90 degrees)

It was observed that design was insensitive to the angular radiation.

No 7: Inner angle of the vertical section.

Bigger: Low resonance point moves higher in frequency but drops down in S_{11}, high resonance point moves lower in frequency and goes up in S_{11}. Total bandwidth decreases.

Sharpen: Low resonance point moves lower in frequency but goes up in S_{11}, high resonance point moves higher in frequency and drops down in S_{11}. Total bandwidth increases.

No 8: Horizontal length (horizontal section only, no tip).

Longer: Low resonance point moves lower in frequency but goes up in S_{11}, high resonance point moves lower in frequency and drops down in S_{11}. Total bandwidth decreases.

Shorter: Low resonance point moves higher in frequency but drops down in S_{11}, high resonance point moves higher in frequency and goes up in S_{11}. Total bandwidth increases.

No 9: Outer angle of the horizontal section.

Bigger: Low resonance point moves higher in frequency but drops down in S_{11}, high resonance point moves lower in frequency and goes up in S_{11}. Total bandwidth decreases.

Sharpen: Low resonance point moves lower in frequency but goes up in S_{11}, high resonance point moves higher in frequency and drops down in S_{11}. Total bandwidth increases.

No 10: Length of the bottom bend.

Longer: Low resonance point moves lower in frequency but goes up in S_{11}, high resonance point moves lower in frequency and drops down in S_{11}. Total bandwidth increases.

Shorter: Low resonance point moves higher in frequency but drops down in S_{11}, high resonance point moves higher in frequency and goes up in S_{11}. Total bandwidth decreases.

No 11: First bend angle (vertical plane bend).

Bigger: Low resonance point moves higher in frequency but goes up in S_{11}, high resonance point moves higher in frequency and goes up in S_{11}. Total bandwidth decreases.

Smaller: Low resonance point moves lower in frequency but drops down in S_{11}, high resonance point moves lower in frequency and drops down in S_{11}. Total bandwidth increases.

No 12: Top to ground height.

Higher: Low resonance point moves higher in frequency but drops down in S_{11}, high resonance point moves higher in frequency and drops down in S_{11}. Total bandwidth increases.

Lower: Low resonance point moves lower in frequency but goes up in S_{11}, high resonance point moves lower in frequency and goes up in S_{11}. Total bandwidth decreases.

No 13: Half gap length.

Longer: Low resonance point moves lower in frequency but goes up in S_{11}, high resonance point moves higher in frequency and drops down in S_{11}. Total bandwidth increases.

Shorter: Low resonance point moves lower in frequency but drops down in S_{11}, high resonance point moves lower in frequency and goes up in S_{11}. Total bandwidth decreases.

No 14: Length of the tip.

Longer: Low resonance point moves higher in frequency but drops down in S_{11}, high resonance point moves lower in frequency and goes up in S_{11}. Total bandwidth decreases.

Shorter: Low resonance point moves lower in frequency but goes up in S_{11}, high resonance point moves higher in frequency and goes down in S_{11}. Total bandwidth increases.

No 15: Outer angle of the tip.

Bigger: Low resonance point moves higher in frequency but drops down in S_{11}, high resonance point moves lower in frequency and goes up in S_{11}. Total bandwidth decreases.

Sharpen: Low resonance point moves lower in frequency but goes up in S_{11}, high resonance point moves higher in frequency and drops down in S_{11}. Total bandwidth increases.

4.2 Experimental Procedure and Results

Prototype antennas were built based on the simulations. Layout of RFID and GPS antenna are shown in Figure 4.14 and Figure 4.15.

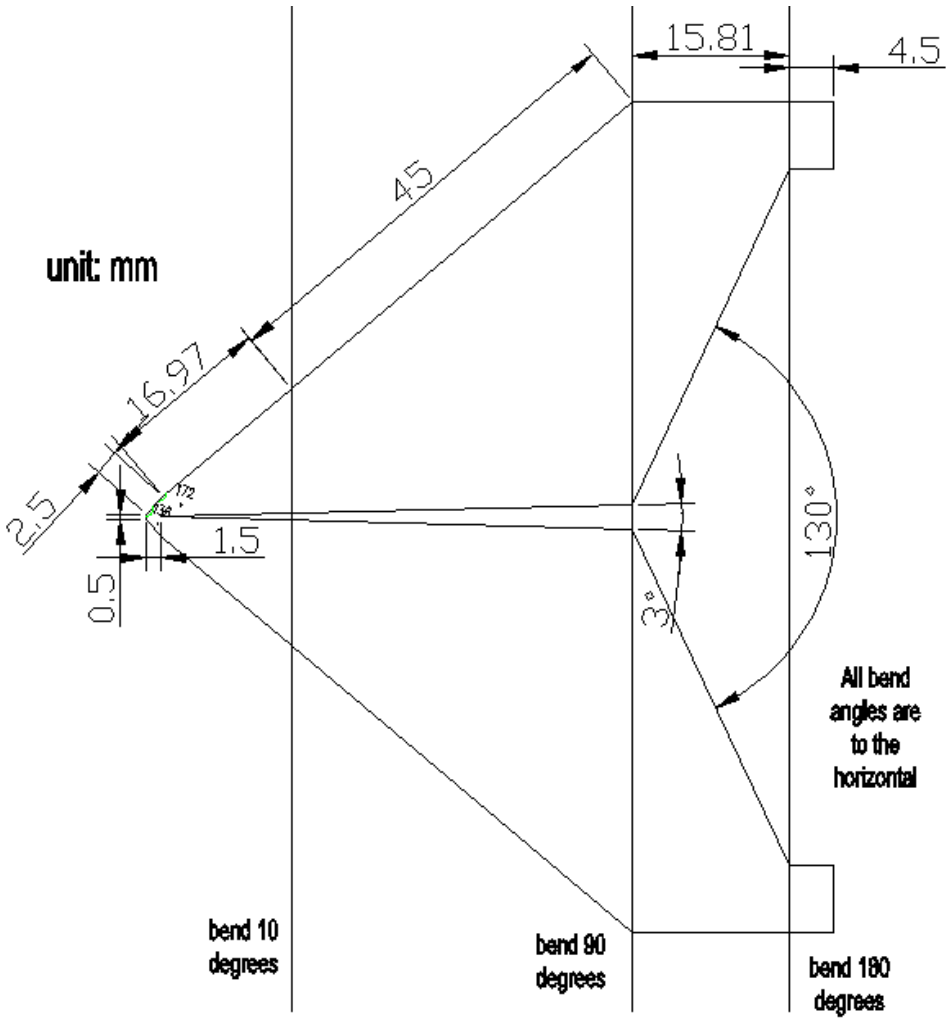

Figure 4.14 Layout of bent bow tie antenna for RFID.

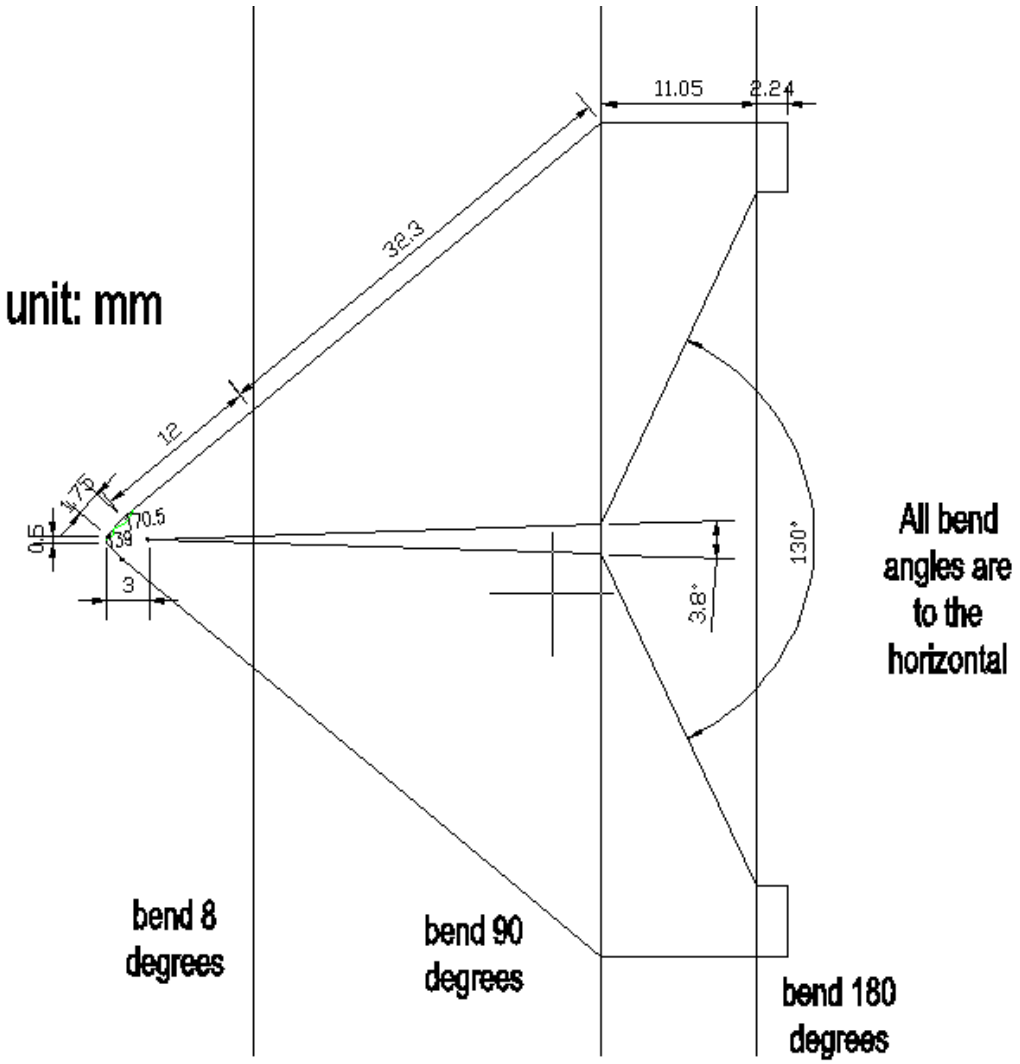

Figure 4.15 Layout of bent bow tie antenna for GPS.

Antennas are fed by a hybrid quadrature coupler. Return loss is tested by vector network analyzer. The prototype antenna under test is shown in Figure 4.16.

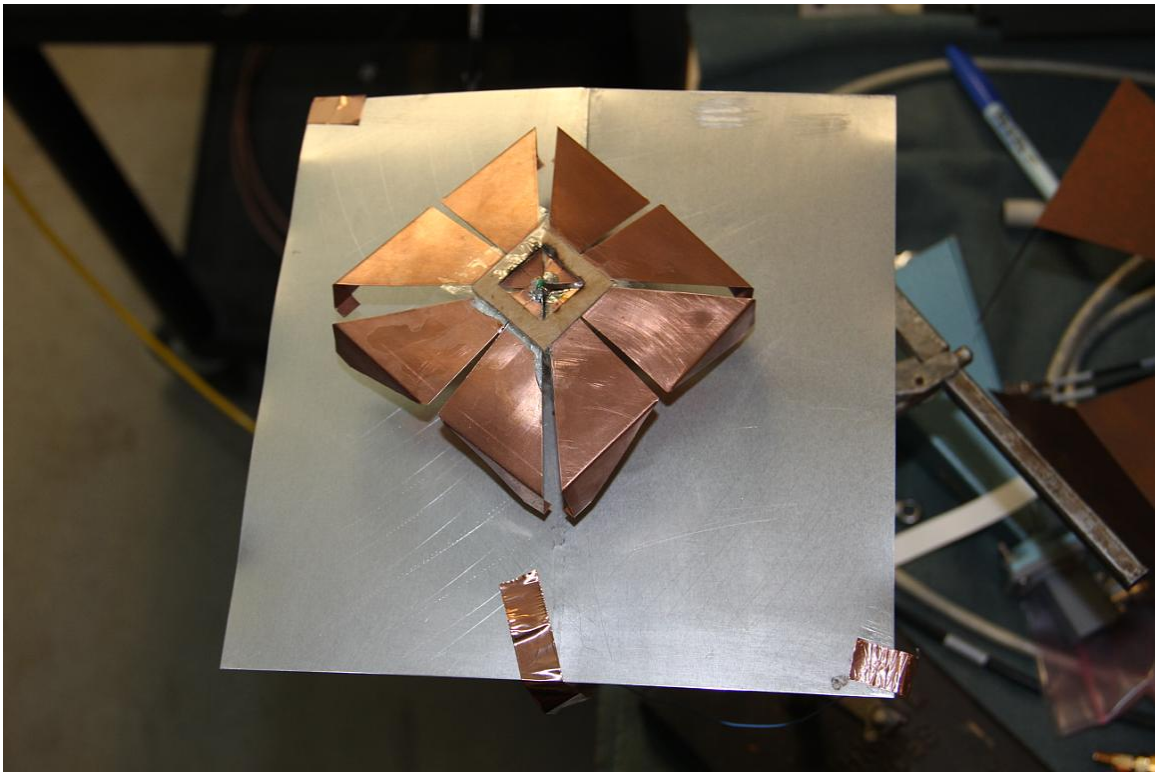

Figure 4.16 (a) Return loss test setup for RIFD antenna.

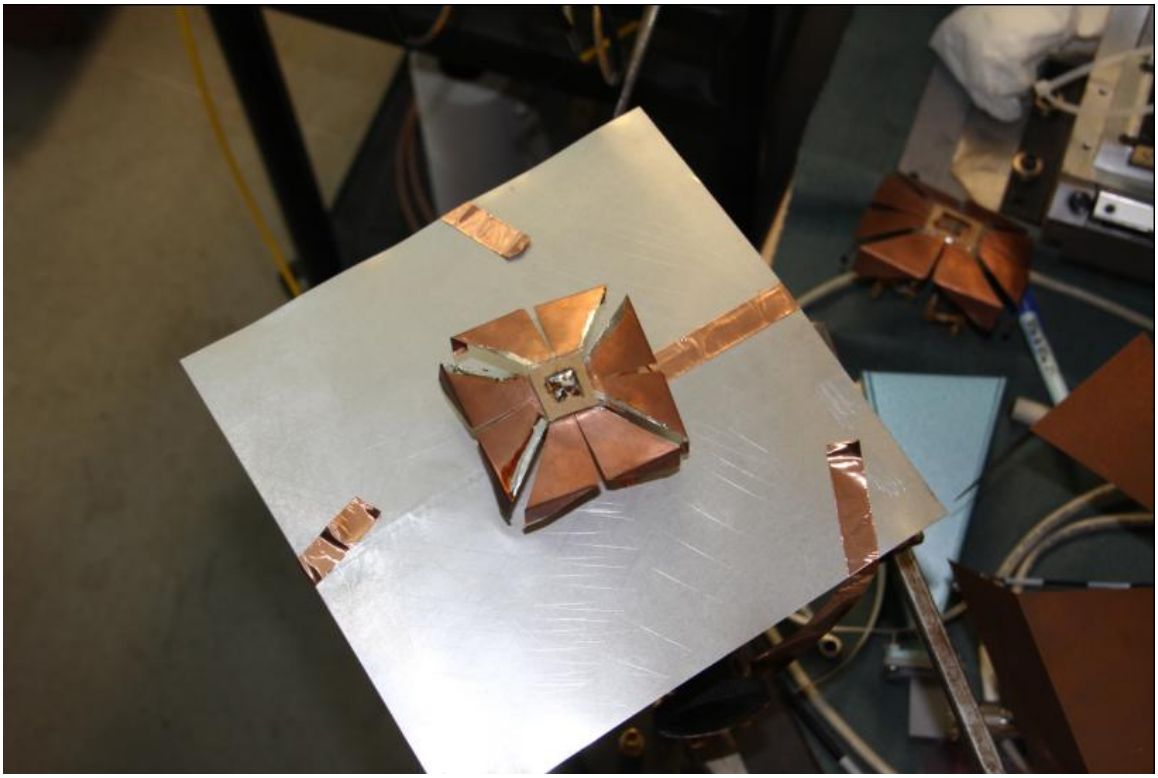

Figure 4.16 (b) Return loss test setup for GPS antenna.

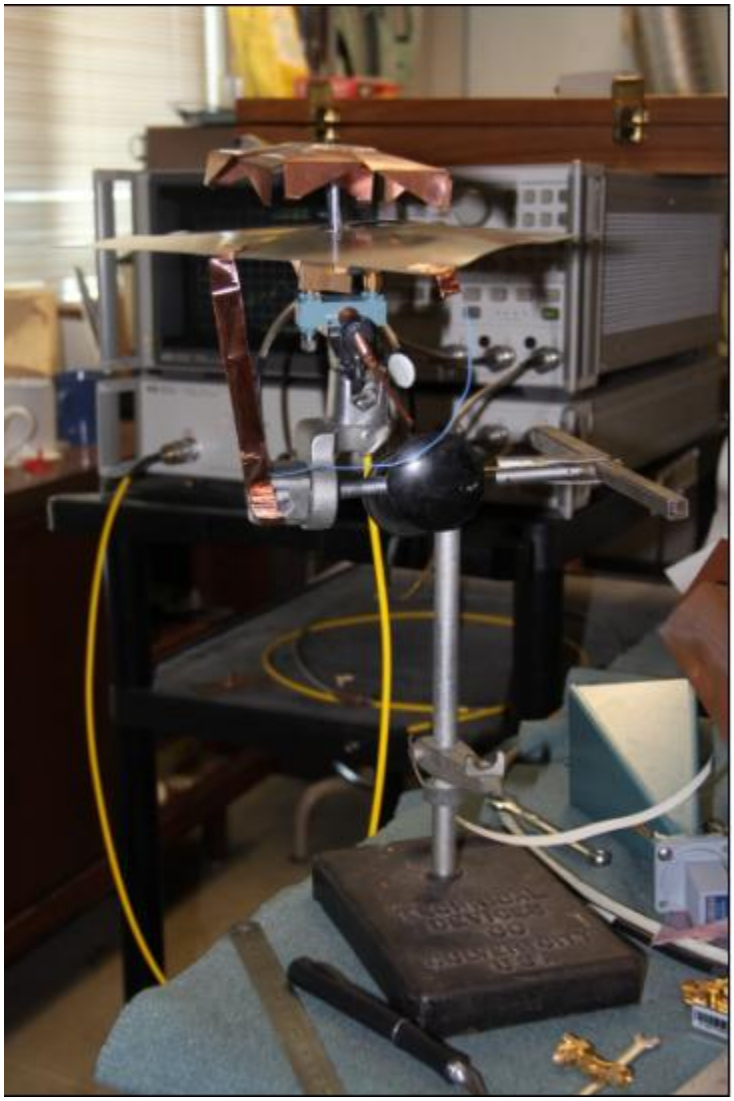

Figure 4.16 (c) Return loss test setup for RIFD antenna.

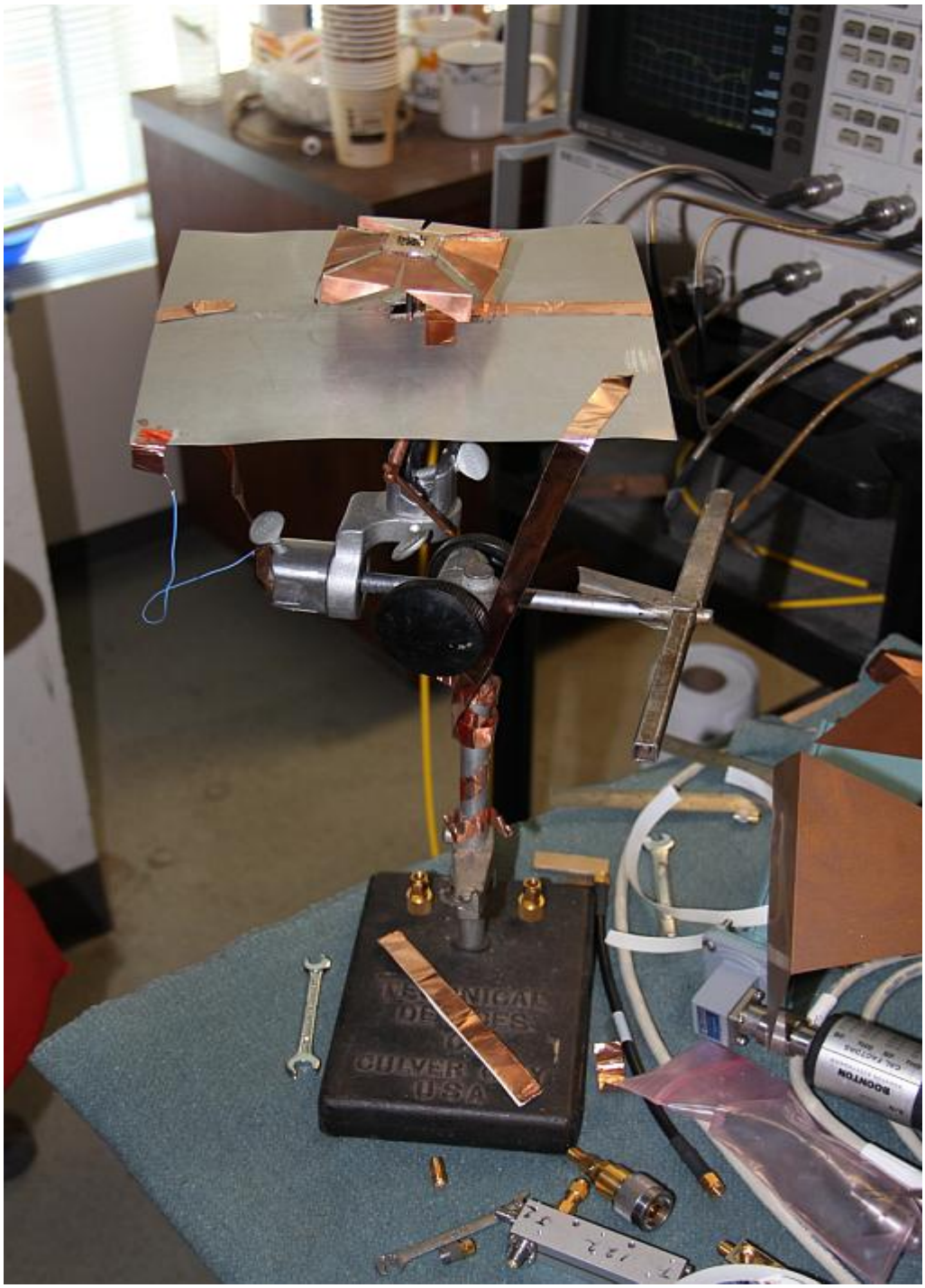

Figure 4.16 (d) Return loss test setup for GPS antenna.

Return loss test results for RFID and GPS antennas are shown in Figure 4.17 and Figure 4.18

Figure 4.17 Return loss test results for RFID antenna.

Figure 4.18 Return loss test results for GPS antenna.

In Figure 4.17, the return loss at the center frequency 950 MHz is about -28 dB, and it shows the return loss in the whole band from 850 MHz to 1050 MHz is lower than -20 dB. In Figure 4.18, the return loss at the center frequency 1386.5 MHz is about -18 dB, and the return loss over the whole band is lower than -15 dB. The test results show that the whole design is very successful.

4.3 Comparison with Other Antennas

In order to show that the new designed bent bow tie antenna for RFID and GPS applications is worthy and advanced, a comparison between the new designed RFID and GPS antenna and the antennas for RFID or GPS application in the market is shown in Tables 4.1 and 4.2.

Table 4.1 Comparison of RFID tag Reader Antennas

Name	Dimensions (cm)	Frequency range (MHz)	Gain (dB)	Front-to-Back ratio (dB)	Beam width
New Bent Bow Tie RFID Antenna	10.0×10.0×2.2	850-1050	6.75	15.35	80 degrees at 3.5 dB
IA33A INTELLITAG	25.9×25.9×3.8	902-928	7	18	65 degrees at 3 dB
AvalLAN wireless 6 dBi indoor antenna	15.0×15.0×4.0	890-960	6.5	12	
Laird Tech S8656-X, Special Application Antennas	19.2×19.2×2.4	865-870	6		80 degrees at 3 dB
Poynting Patch A 0025 Antenna	24.5×23.5×4	860-960	7		

Additional comparison of VSWR and S_{11} between new bent bow tie RFID antenna and Poynting Patch A 0025 antenna are shown in Figure 4.19 and Figure 4.20.

Table 4.2 Comparison of GPS Antennas

Name	Dimensions (cm)	Frequency range (MHz)		Gain (dB)	
		L1	L2	L1	L2
New Bent Bow Tie GPS Antenna	7.3×7.3×1.5	1217.4-1237.8 (20.4)	1528.1-1607.8 (79.7)	6.65	8.26
ALLICOM SB240 Marine GPS Antenna	12.0×12.0×20.65		1575.42±10	4	
GPS SOURCE L1/L2 DARG ANTENNA	6.6×6.6×2.4	1212.6-1242.6 (30)	1560.5-1590.5 (30)	4	7
GPS SOURCE RUGGEDIZED L1/L2 GPS PASSIVE ANTENNA	6.6×6.6×2.4	1217.5-1237.8 (20.3)	1565-1586 (21)	5	5

Data from the above Tables 4.1 and 4.2 suggest that comparable gain performance has reached for almost half size in dimensions for RFID antenna, and for GPS antenna, with comparable size, better gain has been obtained. Further experimental characterization is still in progress. The proposed antenna yields excellent bandwidth and impedance match over that bandwidth.

Figure 4.19 VSWR measurement for new bent bow tie RFID antenna (green) and Poynting Patch A 0025 antenna (blue).

Figure 4.20 S_{11} measurement for new bent bow tie RIFD antenna (green) and Poynting Patch A 0025 antenna (blue).

CHAPTER 5

CONCLUSIONS

Moxon based RFID and GPS antennas were proposed, Extensive numerical simulations based on optimization of various parameters on the antenna structure were carried out to achieve higher gain, wide band impedance match, high cross-polarization and low profile. Prototype antennas were built and tested confirming good agreements between simulation and experimental results. Furthermore, prototype antennas were compared with commercial counterparts and were observed that RFID tag reader antenna was almost 4 times smaller in physical dimensions for the comparable gains. Also the bandwidth of the prototype antenna was significantly wider. In case of GPS antenna the overall gain was observed to increase for the comparable dimensions.

Further investigation of how to improve the performance of the antenna can be done by adding more vertical arms, making more bends along the horizontal part or adding folded elements [12].

REFERENCES

[1] I. Tekin, O. Manzhura and E. Niver, "Broadband Circularly Polarized Antennas for UHF SATCOM," *IEEE General Assembly and Scientific Symposium, 2011 XXXth URSI*, 13-20 Aug. 2011.

[2] L. Moxon, *HF Antennas for ALL Locations*, 2nd Edition, Radio Society of Great Britain, UK, 2002.

[3] K. Finkenzeller, *RFID Handbook,* John Wiley, Hoboken NJ, 1999.

[4] G. Marrocco, "The Art of UHF RFID Antenna Design: Impedance-Matching and Size-Reduction Techniques," *IEEE Antennas and Propagation Magazine*, vol. 50, No.1, 1045-9243, 2008.

[5] B.W. Parkinson and J.J. Spilker Jr., "Global Positioning System: Theory and Applications," *AIAA*, vol.1 &2, Washington, D.C., 1996.

[6] R.S. Elliott, *Antenna Theory and Design*, Prentice-Hall, Inc., Englewood Cliffs, New Jersey 07632.

[7] F. Schwering, "Workshop on Electrically Small Antennas: Background and Purpose." *Proceedings of the ECOM-ARO Workshop on Electrically Small Antennas*, Fort Monmouth, NJ May 6-7, 1976.

[8] L.J. Chu, "Physical Limitations on Omni-Directional Antennas," *J. Appl. Phys.*, vol. 19, pp1163-1175, 1948.

[9] R.M. Fano, "Theoretical limitations on the broadband matching of Arbitrary Impedance." *J.Franklin Inst*, vol.249, pp.58-83,139-154, Jan, Feb, 1950.

[10] L.J. Chu, "Physical Limitations on Omni-Directional Antennas," Technical report N0.64, Research Laboratory of Electronics, MIT, May 1, 1948.

[11] A.K. Skrivervik and J.F. Zürcher, "Electrically Small Antenna Design," Ecole Polytechnique Fédérale de Lausanne, CH-1015 Lausanne, Switzerland Internet: http://www.its.bldrdoc.gov/isart/art08/slides08/tutorial_skr_a-08.pdf, [Apr.13, 2012].

[12] M. Nagatoshi, S. Tanaka, S. Horiuchi and H. Morishita, "Downsized Bow-Tie Antenna with Folded Elements," *IEICE trans electron*, vol. E93-C, no7, July. 2010.

[13] Internet: http://www.ansoft.com/products/hf/hfss/ [Apr. 13, 2012].